



## Spatiotemporal inhomogeneity of total column NO<sub>2</sub> in a polluted urban area inferred from TROPOMI and Pandora intercomparisons

Jong-Uk Park, Jin-Soo Park, Daniel Santana Diaz, Manuel Gebetsberger, Moritz Müller, Lena Shalaby, Martin Tiefengraber, Hyun-Jae Kim, Sang Seo Park, Chang-Keun Song & Sang-Woo Kim

To cite this article: Jong-Uk Park, Jin-Soo Park, Daniel Santana Diaz, Manuel Gebetsberger, Moritz Müller, Lena Shalaby, Martin Tiefengraber, Hyun-Jae Kim, Sang Seo Park, Chang-Keun Song & Sang-Woo Kim (2022) Spatiotemporal inhomogeneity of total column NO<sub>2</sub> in a polluted urban area inferred from TROPOMI and Pandora intercomparisons, *GIScience & Remote Sensing*, 59:1, 354-373, DOI: [10.1080/15481603.2022.2026640](https://doi.org/10.1080/15481603.2022.2026640)

To link to this article: <https://doi.org/10.1080/15481603.2022.2026640>



© 2022 The Author(s). Published by Informa UK Limited, trading as Taylor & Francis Group.



[View supplementary material](#)



Published online: 02 Feb 2022.



[Submit your article to this journal](#)



Article views: 999



[View related articles](#)



[View Crossmark data](#)

## Spatiotemporal inhomogeneity of total column NO<sub>2</sub> in a polluted urban area inferred from TROPOMI and Pandora intercomparisons

Jong-Uk Park<sup>a</sup>, Jin-Soo Park<sup>b</sup>, Daniel Santana Diaz<sup>c</sup>, Manuel Gebetsberger<sup>c</sup>, Moritz Müller<sup>c,d</sup>, Lena Shalaby<sup>e</sup>, Martin Tiefengraber<sup>c,d</sup>, Hyun-Jae Kim<sup>b</sup>, Sang Seo Park<sup>f</sup>, Chang-Keun Song<sup>f</sup> and Sang-Woo Kim<sup>a</sup>

<sup>a</sup>School of Earth and Environmental Sciences, Seoul National University, Seoul, Korea; <sup>b</sup>Climate and Air Quality Research Department, National Institute of Environmental Research, Incheon, Korea; <sup>c</sup>LuftBlick, Innsbruck, Austria; <sup>d</sup>Department of Atmospheric and Cryospheric Sciences, University of Innsbruck, Innsbruck, Austria; <sup>e</sup>NASA Goddard Space Flight Center, Greenbelt, MD, USA; <sup>f</sup>School of Urban and Environmental Engineering, Ulsan National Institute of Science and Technology, Ulsan, Korea

### ABSTRACT

The spatiotemporal inhomogeneity of the total column NO<sub>2</sub> amounts (TCN) in the Seoul Metropolitan Area (SMA), Korea, was quantitatively assessed through year-round (October 2019–May 2021) TROPOMI and ground-based Pandora measurements. The average TCN over the SMA was comparable to that of major Chinese megacities, being consistently high (> 0.8 DU; Dobson Unit) during the daytime (10–17 local standard time). The autocorrelation scores of the Pandora-measured TCNs demonstrated high temporal variability attributed to the spatial inhomogeneity of NO<sub>2</sub> emissions within the SMA and near-surface advection. Accordingly, the adequate temporal collocation range for Pandora measurements for the intercomparison with the satellite sensors was considered to be ± 5 min to avoid significant uncertainty from the temporal variability (RMSE < 0.1 DU, R<sup>2</sup> > 0.96). TROPOMI showed better agreement with conventionally collocated Pandora measurements (0.73 < R<sup>2</sup> < 0.76, 26–29% negative bias) than the other two satellite sensors (OMI and OMPS) attributed to its highest spatial resolution. The application of the wind-based collocation revealed that the TROPOMI showed a greater negative bias on the upwind side, which was less affected by anthropogenic emissions from the urban area, than the downwind side, and the increasing distance of the TROPOMI pixel from Pandora was the most critical factor deteriorating the intercomparison scores. The FRESCO-S TROPOMI cloud algorithm update to FRESCO-wide yielded a general increase in TROPOMI TCN, especially in the partially cloudy pixels, leaving only 11% (downwind) and 29% (upwind) negative bias from coincident Pandora measurements. Furthermore, the wind-based collocation method revealed the spatial distribution pattern of NO<sub>x</sub> (NO + NO<sub>2</sub>) emissions in the SMA, with significant emission sources in the northeastern and southeastern sides of the ground-based Pandora site in Seoul.

### ARTICLE HISTORY

Received 10 August 2021  
Accepted 26 December 2021

### KEYWORDS

TROPOMI; Pandora; total column NO<sub>2</sub>; spatiotemporal variability; Seoul metropolitan area


## 1. Introduction

Nitrogen dioxide (NO<sub>2</sub>) is one of the most well-known anthropogenic gaseous pollutants that can cause serious health problems (Gaffin et al. 2018; Jo et al. 2021; Kampa and Castanas 2008) and acidification (Bytnerowicz, Omasa, and Paoletti 2007; Jonson et al. 2017) and is a precursor for other atmospheric pollutants, such as ozone and aerosols (Jacob 2000; Richards 1983; Sillman 1999; Xie et al. 2015). NO<sub>2</sub> has substantial natural sources (i.e. soil emission, biomass burning, lightning [Beirle, Huntrieser, and Wagner 2010; Jaeglé et al. 2005; Williams, Hutchinson, and Fehsenfeld 1992]), but anthropogenic emissions from fossil fuel combustion (i.e. vehicles and various industrial activities) are known to be the predominant source in the lower troposphere, especially

in the vicinity of a populated urban area (Kim et al. 2013; van der A et al. 2008). Because of its high photochemical reactivity in the atmosphere, the typical daytime lifetime of NO<sub>2</sub> in a polluted boundary layer is limited to a few hours (Beirle et al. 2011; Liu et al. 2016; Martin et al. 2003). Therefore, the NO<sub>2</sub> concentration near urban and industrial areas is highly variable in time and space given the heterogeneous emissions within cities.

The spatial distribution of the NO<sub>2</sub> vertical column density (VCD; total column NO<sub>2</sub> amounts; hereafter, TCN) has been monitored from hyperspectral sensors onboard the low Earth orbit (LEO) satellites, observing reflected light from the atmosphere and the Earth's surface. Since the first differential optical absorption spectroscopy (DOAS [Platt and Stutz 2008])-based TCN

**CONTACT** Sang-Woo Kim  [sangwookim@snu.ac.kr](mailto:sangwookim@snu.ac.kr)

 Supplemental data for this article can be accessed [here](#).

© 2022 The Author(s). Published by Informa UK Limited, trading as Taylor & Francis Group.

This is an Open Access article distributed under the terms of the Creative Commons Attribution-NonCommercial License (<http://creativecommons.org/licenses/by-nc/4.0/>), which permits unrestricted non-commercial use, distribution, and reproduction in any medium, provided the original work is properly cited.

retrieval from the space-borne spectrometer Global Ozone Monitoring Experiment (GOME, aboard ERS-2 [Burrows et al. 1997]), successive hyperspectral imagers, such as the Scanning Imaging Absorption Spectrometer for Atmospheric Cartography (SCIAMACHY, aboard Envisat [Bovensmann et al. 1999]), Ozone Monitoring Instrument (OMI, aboard EOS-AURA [Levelt et al. 2006, 2018]), GOME-2 (aboard MetOp-A/B/C [Liu et al. 2019; Munro et al. 2016]), and Ozone Mapping and Profiler Suite (OMPS, aboard Suomi-NPP and JPSS-1 [Seftor et al. 2014]), have monitored global TCN from space. However, the previous generation of instruments enumerated above cannot resolve the high spatial variability and steep gradient of NO<sub>2</sub> near major source regions. The coarse spatial resolution of imagers and the inherent uncertainty in the air mass factor (AMF) restrained from capturing urban NO<sub>2</sub> plumes, significantly underestimating TCN near the polluted source (i.e. urban area) and slightly overestimating it over the peripheries (Broccardo et al. 2018; Herman et al. 2009, 2018, 2019; Ialongo et al. 2016; Kim et al. 2016; Nowlan et al. 2016, 2018; Valin et al. 2011a, 2011b). The Tropospheric Monitoring Instrument (TROPOMI, aboard Sentinel-5P [Veefkind et al. 2012]), launched in October 2017, opened new horizon monitoring regional to local TCN from space, attributed to its significantly enhanced spatial resolution (3.5 × 5.5 km at nadir) compared to its predecessors. Therefore, TROPOMI TCN products are being widely applied to evaluate and construct emission inventories, identify small-scale plumes near point sources, estimate surface concentrations at high spatial resolutions, and assess NO<sub>2</sub> variabilities in urban areas (Beirle et al. 2019; Goldberg et al. 2019; Griffin et al. 2019; Ialongo et al. 2020, Kim et al. 2020a; Wang et al. 2021; Zhu et al. 2021).

TROPOMI NO<sub>2</sub> products are routinely validated from the Validation Data Analysis Facility (VDAF) of the Sentinel-5P Mission Performance Center (MPC) in collaboration with ground-based networks, such as the Pandora Global Network (PGN; Pandora spectrometers) and Network for the Detection of Atmospheric Composition Change (NDACC; MAX-DOAS and ZSL-DOAS spectrometers), and corroborating in-depth initial validation studies have shown promising results, meeting the pre-launch mission requirements on most occasions (Verhoelst et al. 2021). However, even the high-resolution TROPOMI struggles to accurately estimate the TCN near the polluted emission sources, underestimating the tropospheric NO<sub>2</sub> concentration beyond the target accuracy (Griffin et al. 2019; Ialongo et al. 2020;

Verhoelst et al. 2021; Zhao et al. 2020). It has been reported that reducing the uncertainty of AMF by improving the resolution of chemical transport models (CTMs) and incorporating more accurate inputs (i.e. aerosols and clouds) into the radiative transfer models alleviate the underestimation of TROPOMI TCN in the vicinity of emission hot spots (Ialongo et al. 2020; Kim et al. 2016; Liu et al. 2020; Zhao et al. 2020). Meanwhile, the spatiotemporal variability of NO<sub>2</sub> in an urban area can still be a significant source of discrepancy between satellite and ground-based measurements (Judd et al. 2019; Park et al. 2020; Tzortziou et al. 2015). Therefore, a more comprehensive comparison of TROPOMI TCN with accurate ground-based reference measurements (i.e. Pandora spectrometer and MAX-DOAS) is required to assess the error due to the spatiotemporal variability of NO<sub>2</sub> within the urban area and obtain a strategy for satellite validation.

In this study, we investigated the spatiotemporal variability of TCN from year-round Pandora and TROPOMI observations in the Seoul Metropolitan Area (SMA), which is one of the locations with the highest anthropogenic NO<sub>x</sub> (NO + NO<sub>2</sub>) emissions and concentrations in the world (Herman et al. 2019; Jeong and Hong 2021; Judd et al. 2018; Kim et al. 2020a; Vellingiri et al. 2015). The general characteristics of the TCN in the SMA are introduced, revealing the distinctiveness of SMA among other regions in South Korea and the diurnal variation of TCN. The temporal variability of the TCN in the SMA is estimated from high-frequency Pandora observations, and the optimal temporal collocation range for satellite-Pandora intercomparison is suggested. Moreover, spatial variability and the heterogeneity of TCN distribution are quantified using the wind-based collocation method (Zhao et al. 2020), consolidating its utility for future applications with geostationary (GEO) satellites, such as the Geostationary Environment Monitoring Spectrometer (GEMS, aboard GK-2B [Kim et al. 2020b]).

## 2. Data and methodology

### 2.1. Pandora total column NO<sub>2</sub> observations

A ground-based hyperspectral Pandora instrument (Pandora 1S model) measures radiance at 280–525 nm with a nominal spectral resolution of 0.6 nm and four times oversampling from its temperature-controlled (20°C) symmetric Czerny–Turner system

Avantes spectrometer with  $2048 \times 64$  pixels Hamamatsu charge-coupled device (CCD) (Herman et al. 2015, 2018). Pandora has a nominal  $1.5^\circ$  field of view (FOV;  $2.5^\circ$  with a diffuser) and can measure both direct sun and sky radiance with its vast dynamic range ( $\sim 10^7$ ) owing to the variant exposure time (2.4–4000 ms) and neutral density filters, which attenuate the intensity (Herman et al. 2015, 2018).

Pandora TCN retrieval uses direct sun observations to make the calculation much more accurate and less expensive by assuming geometric AMF (Cede et al. 2006; Herman et al. 2009) and disregarding the Ring effect from rotational Raman scattering (Langford et al. 2007). The slant column density (SCD) of  $\text{NO}_2$  was calculated by adding differential SCD (dSCD) and the SCD of the reference spectrum ( $\text{SCD}_{\text{ref}}$ ). The reference spectrum is determined by the low solar zenith angle measurement(s) from each respective Pandora spectrometer to minimize instrumental uncertainties. The difference between the measured and reference spectrum is used for DOAS fitting to calculate the dSCD, with a fitting window of 400–440 nm and absorption cross-section of  $\text{O}_3$  (225 K [Serdyuchenko et al. 2014]) and  $\text{NO}_2$  (254.5 K [Vandaele et al. 1998]). The  $\text{SCD}_{\text{ref}}$  is retrieved based on a modified Langley extrapolation (MLE) method, assuming a hypothetical day with the lowest  $\text{NO}_2$  and invariant upper layer (free troposphere and stratosphere) column  $\text{NO}_2$  (Herman et al. 2009). The uncertainty of Pandora TCN is known to be approximately 0.05 DU (Dobson Unit; equivalent to  $2.687 \times 10^{16}$  molecules  $\text{cm}^{-2}$ ; below 0.1 DU even in highly polluted cases), which is mainly attributable to the uncertainty of the  $\text{SCD}_{\text{ref}}$  estimated from the MLE method as well as the temperature dependency of the  $\text{NO}_2$  absorption cross-section (Herman et al. 2009, 2018, 2019).

In this study, we used TCN measured from two collocated Pandoras (P149 and P163; <https://www.pandonia-global-network.org/>) between October 2019 and May 2021 at Seoul National University (Seoul-SNU;  $37.46^\circ\text{N}$ ,  $126.95^\circ\text{E}$ , 110 m above sea level) located on the southern side of Seoul (Kim et al. 2021; Park et al. 2018). Observations were made in a standard PGN high-speed mode schedule ( $\sim 90$  s per cycle), allocating 20 s per observation mode, but occasional sky scanning leaves a gap ( $\sim 10$  min) between consecutive TCN observations. The BlickP processor version 1.7.28 with “rnvs1” code was utilized for TCN retrieval, and only the data points with high quality (L2 data quality flag = 0 or 10) were

accounted for in the analysis. Additional Pandora observations from the KORUS-AQ campaign (Herman et al. 2018) were included in this study.

## 2.2. Satellite total column $\text{NO}_2$ observations (TROPOMI, OMI, and OMPS)

TROPOMI is a push-broom-type hyperspectral imaging sensor aboard the Sentinel-5 Precursor satellite, observing UV/VIS (270–500 nm), NIR (675–775 nm), and SWIR (2305–2385 nm) bands with four separate spectrometers (UV, UVIS, NIR, and SWIR [Kleipool et al. 2018; Veefkind et al. 2012]). The wide FOV ( $108^\circ$ ) and flight altitude (824 km) yield a sufficient swath (2600 km) for daily global coverage, providing 1–2 observations per day over the SMA between 12 and 15 local standard time (LST; 03–06 UTC). The CCD detector effectively using 862 pixels across-track delivers  $3.5$  (across-track)  $\times$   $5.5$  km (along-track; switched from 7 km since 6 August 2019) resolution at nadir with a sufficiently high signal-to-noise ratio (SNR) in UVIS bands (Eskes et al. 2020; Kleipool et al. 2018).

The TROPOMI  $\text{NO}_2$  retrieval algorithm was developed by the Royal Netherlands Meteorological Institute (KNMI) based on the Dutch OMI  $\text{NO}_2$  (DOMINO) retrieval algorithm (Boersma et al. 2011) and some improvements from the Quality Assurance for Essential Climate Variables (QA4ECV) project (Boersma et al. 2018; van Geffen et al. 2015, 2019). The SCD of  $\text{NO}_2$  was retrieved from DOAS fitting over 405–465 nm and then separated into tropospheric and stratospheric parts based on data assimilation in the TM5-MP CTM (Williams et al. 2017) before applying the respective AMF to convert it into the VCD. The AMF was calculated based on a look-up table of altitude-dependent AMFs and the vertical distribution of  $\text{NO}_2$  from the TM5-MP CTM ( $1^\circ \times 1^\circ$  grid; van Geffen et al. 2019). The surface albedo was adopted from OMI climatology ( $0.5^\circ \times 0.5^\circ$  grid; Kleipool et al. 2008) and GOME-2 measurements (Tilstra et al. 2017), while cloud pressure from the TROPOMI Fast Retrieval Scheme for Clouds from the Oxygen A-band (FRESCO) and cloud radiance fraction (CRF) from the  $\text{NO}_2$  fitting window ( $\sim 440$  nm) were utilized for the calculation (van Geffen et al. 2019). The TROPOMI  $\text{NO}_2$  retrieval algorithm was updated from v1.3 to v1.4 on 28 November 2020 (offline products) with a major update of the FRESCO-S cloud scheme to the FRESCO-wide (Eskes and Eichmann 2020). The update of the FRESCO algorithm resulted in an overall decrease in cloud pressures (Eskes et al. 2020),

especially for low-level clouds, and resolved the cloud height underestimation issue for low-level clouds (Compernelle et al. 2021), decreasing the AMF for cloudy (or heavily aerosol-loaded) pixels, and consequently increasing the NO<sub>2</sub> tropospheric VCD (VCD<sub>trop</sub>) (Eskes et al. 2020).

In this study, offline level 2 NO<sub>2</sub> VCD<sub>sum</sub> (= VCD<sub>trop</sub> + VCD<sub>strat</sub>) (ESA, KNMI 2019) was adopted as the TCN instead of VCD<sub>total</sub> because the additional separation process of SCD<sub>trop</sub> and SCD<sub>strat</sub> using data assimilation reduces the error (van Geffen et al. 2019). TROPOMI pixels with qa\_value ≤ 0.75 were disregarded, which embraced the dismissal of cloudy pixels with a CRF > 0.5. In particular, the average CRF of TROPOMI pixels in this study was 0.08 (99.0% below 0.3), while the TROPOMI footprint size ranged from 20.2 to 76.7 km<sup>2</sup> (35.0 km<sup>2</sup> on average, approximately 1.8 times larger than at the nadir).

OMI is a push-broom-type hyperspectral imager that observes ultraviolet and visible light (270–500 nm) onboard the EOS-AURA satellite. OMI has a CCD detector with 60 spatially co-added pixels, yielding a 13 (along-track) × 24 km (across-track) resolution at the nadir and 2600 km swath (Levelt et al. 2006). TCN data from Making Earth System Data Records for Use in Research Environments (MEASUREs) Multi-Decadal Nitrogen Dioxide and Derived Products from Satellites (MINDS) v1.0 (Lamsal et al. 2020) were utilized in this study. Quality flags were used to select pixels with successful retrievals (vcdQualityFlags divided by 4), which excluded cloudy pixels (effective cloud fraction > 0.3) and pixels affected by row anomalies (Schenkeveld et al. 2017).

OMPS is one of the payloads in the Suomi-NPP satellite, with an overpass time 10–15 min earlier than that of the EOS-AURA satellite (Yang et al. 2014). TCN is retrieved from a direct vertical column-fitting algorithm using spectral observations from the nadir mapper (NM) of the OMPS (Yang et al. 2014; Yang 2017). Because the primary objective of OMPS NM is to observe the column amount of O<sub>3</sub>, it covers 300–380 nm with a spectral resolution of 1 nm, and a coarse spatial resolution (50 × 50 km at nadir) from 35 across-track pixels over a 2800 km swath (Yang et al. 2014; Yang 2017). The TCN from OMPS-NPP NMNO2 L2 data (Yang 2017) was utilized in this study, quality controlled with quality flags and excluded cloudy pixels (radiative cloud fraction > 0.3).

### 2.3. Wind-based collocation of TROPOMI and Pandora measurements

The conventional collocating method of LEO satellites and ground-based instruments utilizes a single satellite pixel that includes the surface location of the ground-based instrument for intercomparison, significantly limiting the number of collocated measurements. In particular, the number of conventionally collocated TCN measurements of TROPOMI and Pandora in the SMA is limited to a maximum of twice a day, which is further filtered out due to cloudy pixels. A limited number of collocated measurements between TROPOMI and Pandora are major hurdles for the comprehensive analysis of the TROPOMI validation. Meanwhile, the wind-based collocating method embracing TROPOMI pixels located upwind or downwind from the Pandora site has shown its utility by significantly increasing the number of coincident measurements between TROPOMI and Pandora (Zhao et al. 2020). Moreover, the high spatial resolution of TROPOMI in combination with the surface wind field enables analysis of the spatial distribution of major NO<sub>x</sub> source regions in the SMA and the effect of near-surface (boundary layer) NO<sub>2</sub> transport.

In this study, we employed ERA5 (ECMWF Reanalysis v5) hourly reanalysis (Hersbach et al. 2018, 2020) wind data averaged over 1000–900 hPa pressure levels and linearly interpolated to the exact location of the Pandora site and TROPOMI overpass time. The TROPOMI pixels rotated based on the wind direction (θ), such that the wind direction was always the same in the rotated coordinate system (i.e. wind aligned to the y-axis from the positive to the negative side). With the tangent plane assumption and coordinate system centered at the Pandora site (i.e. Pandora site located on the point of origin), applying a rotational matrix ( $R(\theta)$ ) to the initial coordinates of the TROPOMI pixel ( $P_{init}(x_i, y_i)$ ; Figure 1a) yielded rotated coordinates ( $P_{rot}(x_r, y_r)$ ; Figure 1b).

$$R(\theta) = \begin{pmatrix} \cos\theta & -\sin\theta \\ \sin\theta & \cos\theta \end{pmatrix} \quad (1)$$

$$P_{rot} \begin{pmatrix} x_r \\ y_r \end{pmatrix} = R(\theta) P_{init} \begin{pmatrix} x_i \\ y_i \end{pmatrix} \quad (2)$$

The upwind ( $y_r > 0$ ) and downwind ( $y_r < 0$ ) sides were determined based on the rotated coordinates, and the pixels with  $x_r$  in between  $\pm \rho$  (tolerance interval) were regarded as a collocated upwind/downwind pixel. The square root of the average TROPOMI footprint area

within the  $\pm 1^\circ$  latitude/longitude domain was adopted as the tolerance interval ( $\rho$ ) of each particular swath ( $\rho_{\text{mean}} = 5.80$  km; ranging from 4.51–8.43 km) so that the nearest TROPOMI pixel to the wind direction line (i.e. y-axis) was selected as a collocated pixel. The air mass travel time was calculated for each collocated TROPOMI pixel by dividing the distance from the Pandora site by the wind speed, and only the pixels with travel times of less than 1 h were regarded in this study to account for the short atmospheric lifetime of  $\text{NO}_2$  in a polluted urban boundary layer. By adding (for upwind pixels) or subtracting (for downwind pixels) the travel time from the TROPOMI overpass time, the coincident time of the Pandora measurement to a particular TROPOMI pixel was calculated and utilized for an intercomparison. The average distance of TROPOMI pixels from Pandora was  $14.20 \pm 8.75$  km in this study, and further details of the wind-based collocation method are available in Zhao et al. (2020).

### 3. Results and discussion

#### 3.1. General features of total column $\text{NO}_2$ in SMA

Despite recent efforts to improve air quality with intense mitigation of anthropogenic pollutants, East Asia remains one of the locations with the highest  $\text{NO}_2$  emissions and concentrations in the world. Observations from the TROPOMI (Figure 2a) pinpoint the primary source regions with exceptionally high TCN; the East Asian megacities (i.e. the Beijing-Tianjin-Hebei (BTH) region, Shanghai, SMA, and

Tokyo), which is typically attributable to their immense population. In particular, the average TROPOMI TCN during the study period in SMA (0.70 DU) is comparable to the BTH and Shanghai regions, soaring up to 0.83 DU in downtown Seoul. Discernible intra-city spatial inhomogeneity and elevated  $\text{NO}_2$  concentrations reaching 120 km on the southeastern side of Seoul are shown in Figure 2b and Supplementary Figure S1, which is a downscaled high-resolution ( $0.01^\circ$  grid in latitude and longitude) TROPOMI TCN composite and the depiction of major arterial roads and their traffic loadings on a nominal weekday, respectively, over the SMA and its outskirts. Specifically, the populated downtown areas of Seoul, major highways and arterial roads, and major satellite cities, such as Seongnam and Suwon, are well-depicted, constituting the spatial inhomogeneity within the SMA, while the  $\text{NO}_2$  transport under prevailing northwesterlies can be inferred from the extended polluted area on the southeastern side.

Figure 3 and Supplementary Figure S2 show the diurnal variation of TCN observed with multiple Pandoras at various locations (Table 1) in South Korea. Pandoras located in Seoul (Olympic Park, Yonsei University, and Seoul-SNU) show distinctively higher TCN compared to other sites, with the diurnal variation resembling a unimodal pattern with consistently high TCN ( $> 0.9$  DU) during the daytime (10–17 LST). The diurnal variation pattern of TCN in this study differed from the previously reported surface  $\text{NO}_2$  concentration in an urban area, which showed a bimodal structure

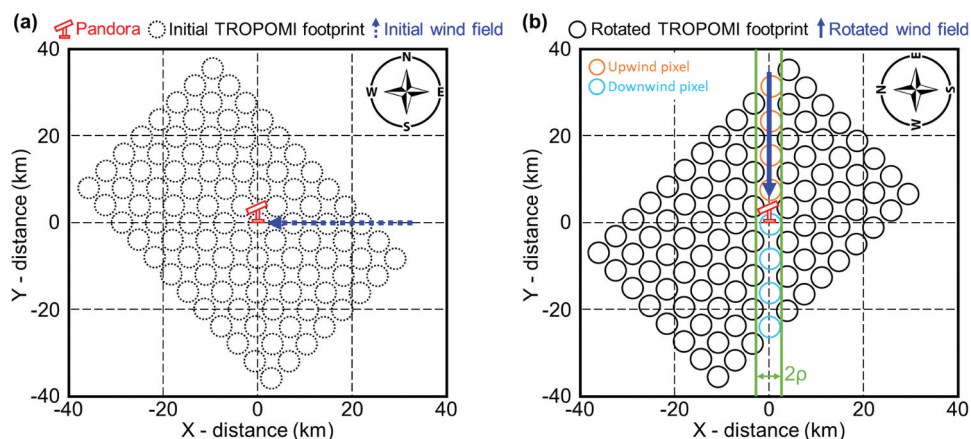


**Figure 1.** Schematic diagram of the wind-based collocation method. (a) Initial TROPOMI pixels (footprints) and wind field, and (b) rotated TROPOMI pixels and wind field assuming a tangent plane under the Pandora centered coordinate. The upwind (orange) and downwind (cyan) TROPOMI pixels of Pandora were selected after the rotation assuming tangent-plane, only if the center of the TROPOMI pixel was in the tolerance range ( $-\rho < x_r < +\rho$ ) (modified from Zhao et al. 2020).

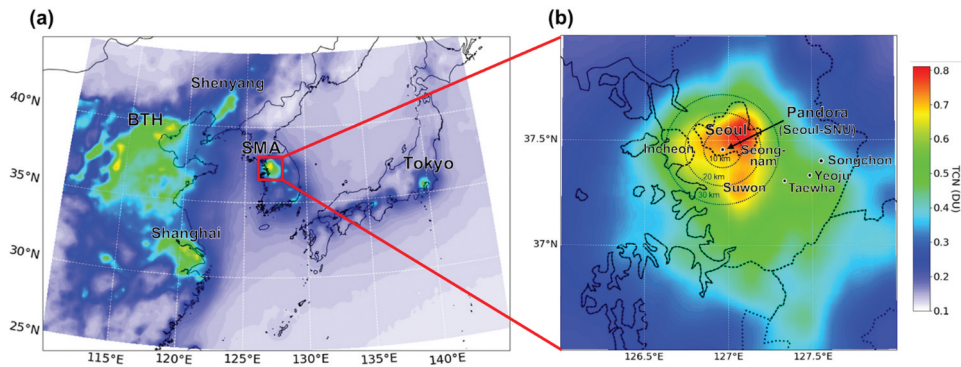


**Figure 2.** Average TROPOMI TCN during the study period (October 2019–May 2021) over (a) East Asia and (b) the Seoul Metropolitan Area (SMA). TROPOMI swath data over SMA domain (b) were downscaled to a high-resolution  $0.01^\circ$  latitude/longitude grid using the interpolation inversely weighted with the distance.

with a local minimum in the afternoon, but was concordant with the TCN reported during the KORUS-AQ campaign (Crawford et al. 2021; Herman et al. 2018). Accordingly, the boundary layer development during the day appears to play a substantial role in the afternoon local minima of surface  $\text{NO}_2$  concentrations in Seoul (Boersma et al. 2009; Crawford et al. 2021; Flynn et al. 2014). Moreover, the conspicuous discrepancy between the average TCN measured by three different Pandoras located within Seoul implies high intra-city inhomogeneity of midday  $\text{NO}_2$  concentrations, but the different observation periods shown in Table 1 should take considerable responsibility for the differences among the three Pandoras. The downwind sites of Seoul (Songchon, Yeoju, and Taehwa; Figure 2b) show a unique diurnal variation

pattern of TCN with an abrupt increase in the evening (after 17 LST), suggesting an impact from a transported plume from Seoul. It is noteworthy that the downwind rural sites of Seoul with no major anthropogenic activities are showing comparable (Songchon and Yeoju) to an even higher (Taehwa) TCN than the other major cities (Ulsan, Busan, and Gwangju) in South Korea, consolidating the importance of the SMA with respect to  $\text{NO}_x$  emissions in South Korea and emphasizes the significance of  $\text{NO}_2$  transport in the SMA. On the other hand, the Global Atmosphere Watch (GAW) regional background site located on the western coast of Korea, Anmyeon Island (Laj et al. 2020), shows TCN of around 0.2–0.3 DU, representing the national background TCN with minimal impact of anthropogenic  $\text{NO}_2$  pollution.

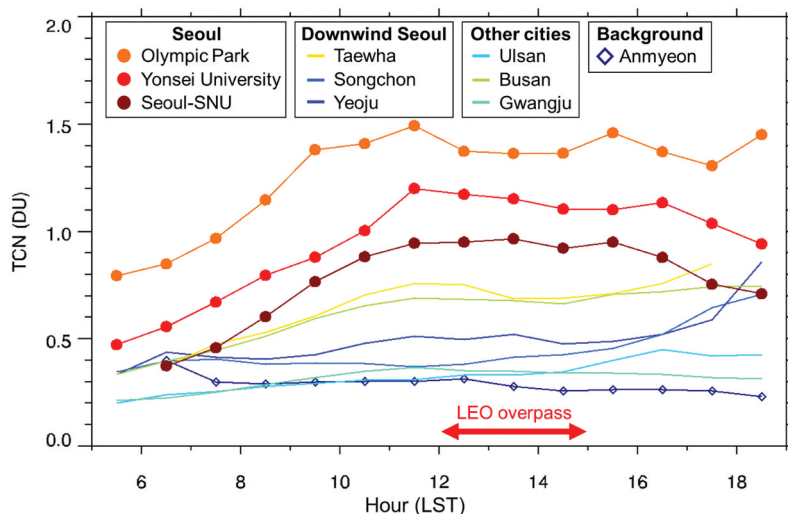


**Figure 3.** Diurnal variation of the TCN observed from Pandora spectrometers at different locations in Korea.

**Table 1.** The observation period of Pandora spectrometers shown in Figure 3.

Pandora no.	Site name	Classification	Data period	Remarks
P163	Seoul-SNU	Seoul (urban)	11 October 2019–31 May 2021	PGN official
P39	Olympic Park	Seoul (urban)	29 April 2016–14 June 2016	KORUS-AQ
P40	Yonsei Univ.	Seoul (urban)	16 May 2016–15 October 2016	KORUS-AQ
P20	Taehwa	Downwind Seoul (rural)	11 April 2016–12 June 2016	KORUS-AQ
P35	Yeoju	Downwind Seoul (rural)	13 May 2016–27 June 2016	KORUS-AQ
P38	Songchon	Downwind Seoul (rural)	10 May 2016–15 June 2016	KORUS-AQ
P150	Ulsan	Metropolitan city (sub-urban)	25 July 2019–4 November 2020	PGN official
P17	Busan	Metropolitan city (urban)	6 April 2016–28 December 2020	PGN official
P26	Gwangju	Metropolitan city (urban)	1 May 2015–17 October 2016	KORUS-AQ
P21	Anmyeon	Background (rural)	31 December 2015–7 April 2016	KORUS-AQ

### 3.2. Temporal variability of total column NO<sub>2</sub> and the conventional collocation

Figure 4a shows the cross-correlation of TCN measured during the collocated period of P149 and P163 using the nearest temporally coincident measurements within the temporal collocation window, whereas the temporal collocation window range from  $\pm 5$  (top) to  $\pm 60$  (bottom) min. The two Pandoras were effectively in conformity with  $R^2 > 0.98$ , root mean square errors (RMSE)  $< 0.06$  DU, and negligible mean bias ( $< 0.01$  DU) throughout the collocation range, which ensures the credibility of Pandora as a high-precision reference ground-based instrument. Moreover, the number of collocated cases remained almost the same with only a small increment with the temporal collocation range enlargement, indicating that the standard high-speed mode observation schedule of PGN (in this case, “uv\_sun\_moon\_sky\_hsm”) ensures sufficiently frequent observation so that the Pandoras make a coincident observation within  $\pm 5$  min on most occasions.

The autocorrelations of TCN calculated after diverse time lags (1–90 min) with  $\pm 1$  min averaging intervals are shown in Figure 4b and Supplementary Figure S3. Both Pandoras show apparent degradation in autocorrelation scores (decreasing  $R^2$  and increasing RMSE) with increasing time lag. In particular, a time lag greater than 5 min cannot ensure  $RMSE < 0.1$  DU and  $R^2 > 0.96$ , which is already far beyond the precision level of Pandora (0.02 DU in Zhao et al. 2020), and 1 h of temporal discrepancy reduces  $R^2$  below 0.7 and RMSE up to 0.3 DU. The rapid decline in  $R^2$  and increase in RMSE indicate high temporal variability of TCN in Seoul during the daytime, so

that a slight enlargement of the temporal collocation interval can induce significant uncertainty. Moreover, the difference in the measurement period of P149 (May 2020–Jun 2020, Nov 2020–May 2021) and P163 (Oct 2019–May 2021, except July 2020) resulted in a slight disagreement in RMSE (higher RMSE in P163), suggesting a possible variation in temporal variability. It is noteworthy to mention that there was an evident linear increasing trend of bias on the positive side with increasing time lag at a rate of approximately 0.05 (P149)–0.065 (P163) DU hr<sup>-1</sup> (Figure S3). Some of this monotonic increase in biases can be explained by diurnal variations in stratospheric column NO<sub>2</sub> during the day, which also exhibits a gradual increase during the daytime attributed to the photolysis of N<sub>2</sub>O<sub>5</sub> (Belmonte Rivas et al. 2014; Gil et al. 2008; Solomon, Russell, and Gordley 1986; Vaughan et al. 2006). However, previous studies by Celarier et al. (2008) and Wang et al. (2020) report only about 0.05 DU increase in stratospheric column NO<sub>2</sub> throughout the daytime (i.e. from sunrise to sunset), which indicates that most of the positive bias is attributable to the increasing TCN in the morning (Figure 3) from intensifying NO<sub>x</sub> emissions rather than the stratospheric variability.

Figure 5 shows a scatterplot comparing collocated TCN measurements from Pandora at Seoul-SNU (P163) and three satellite sensors (TROPOMI, OMI, and OMPS). The conventional collocation (i.e. comparing Pandora with satellite pixel that includes Pandora location) method was employed with different temporal collocation intervals ranging from  $\pm 1$  to  $\pm 90$  min from the satellite overpass time, and the Pandora TCNs measured within the collocation interval were averaged



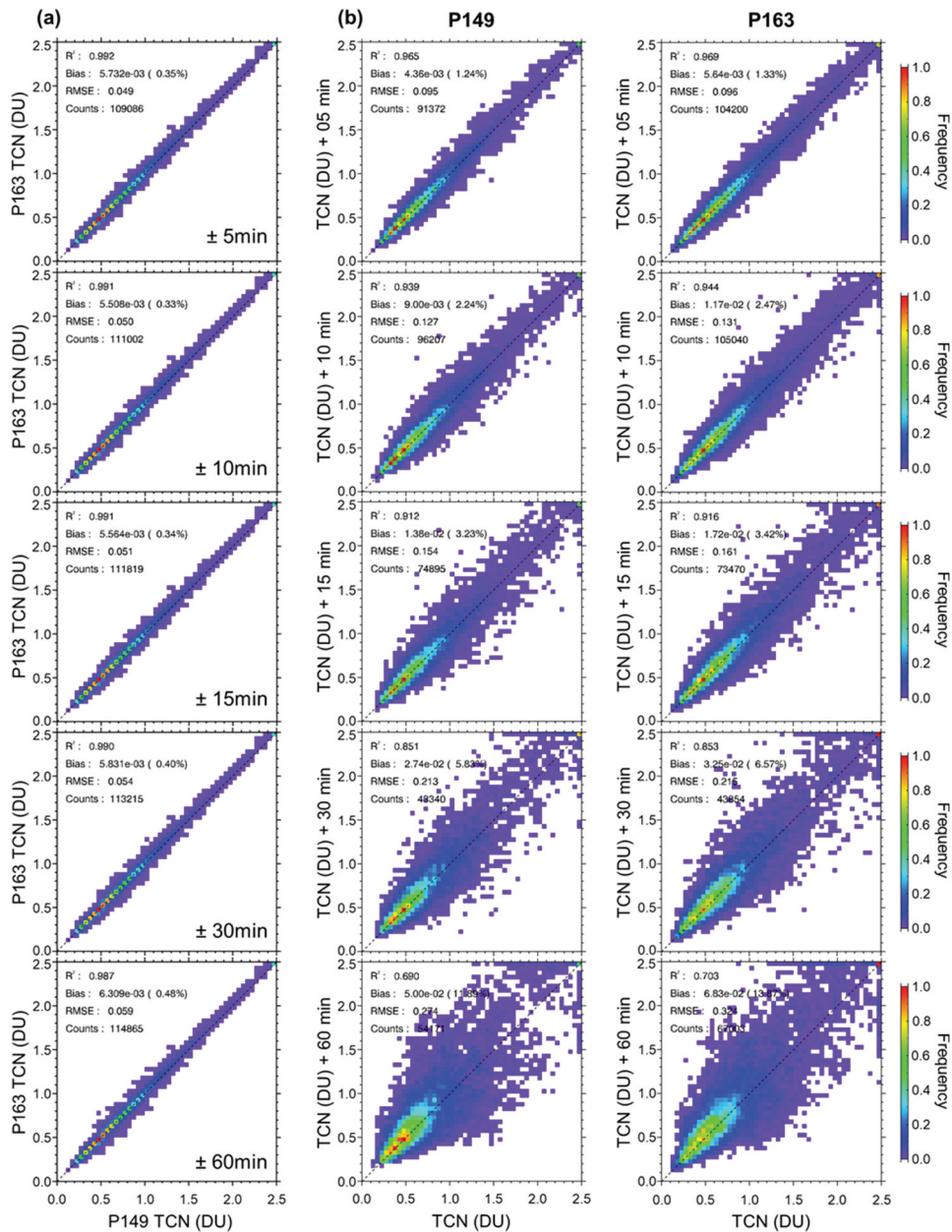


**Figure 4.** (a) Cross-correlation of measured TCN between collocated P149 and P163 at Seoul-SNU with a different temporal collocation range. (b) Autocorrelation of TCN observed from P149 (left) and P163 (right) with different time lags. Units for bias and RMSE are in DU.

for an intercomparison. TROPOMI showed an  $R^2$  value of around 0.72–0.76 throughout the collocation intervals with consistent underestimation (26–29%) and a mean negative bias of 0.21–0.24 DU, while OMI showed a lower correlation ( $0.28 < R^2 < 0.39$ ) and more significant underestimation (37–43%). The relatively lower spatial resolution and sensor degradation (i.e. cross-track striping) of OMI are responsible for the lower intercomparison scores with the Pandora, while the row anomaly issue of OMI resulted in notably less collocated measurements than the TROPOMI.

Meanwhile, OMPS showed the lowest intercomparison scores with Pandora shown by the greatest mean bias (0.49–0.56 DU), RMSE (0.72–0.82 DU), underestimation (67–73%), and the lowest correlation ( $0.06 < R^2 < 0.11$ ), which can be anticipated from its lowest spatial-spectral resolution and the lower sensitivity to the lower atmosphere. This result was consistent with that of previous studies (Griffin et al. 2019; Ialongo et al. 2020; Judd et al. 2019), indicating that the low spatial resolution of satellite sensors, incapable of resolving the sharp gradient of  $\text{NO}_2$  near the urban

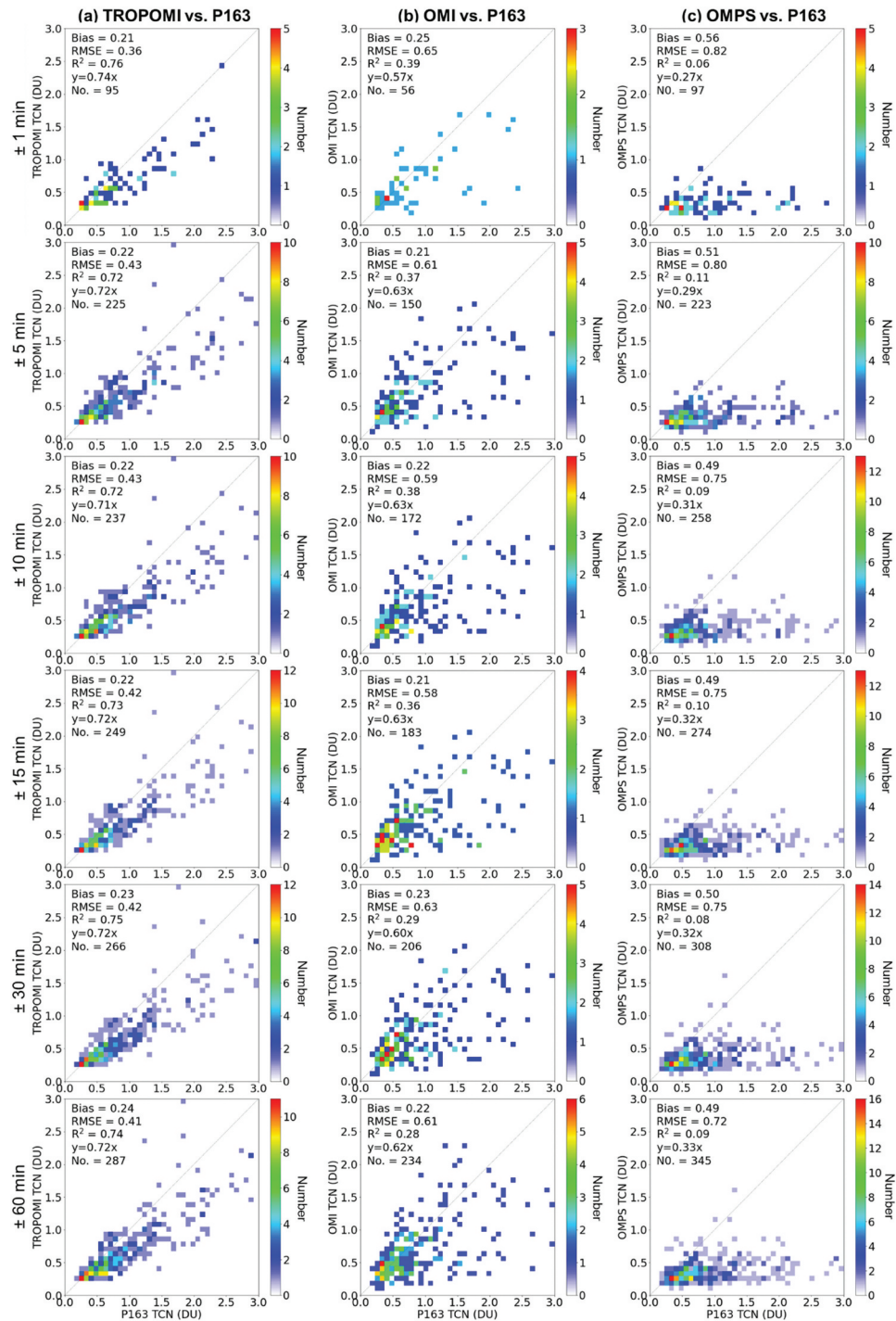


**Figure 5.** Comparison of TCN measured from Pandora (P163) and satellite-borne hyperspectral sensors: (a) TROPOMI, (b) OMI, and (c) OMPS, with different temporal averaging collocation ranges (1–90 min). Units for bias and RMSE are in DU.

area, as a cause of the general satellite TCN underestimation compared to ground-based reference measurements (i.e. Pandora).

It is noteworthy that the autocorrelation scores of Pandora TCN showed evident deterioration with increasing time lag, whereas the intercomparison scores between Pandora and satellite sensors showed minimal

dependency on the temporal collocation interval. The optical path of Pandora's direct sun observation had a small horizontal footprint during the typical overpass time of LEO satellites in the SMA (early afternoon) and can be assumed as a point measurement. However, satellite sensors observe scattered light from a wider area; hence, they inherently have an equivalent effect

of spatial averaging within their pixel footprints. Therefore, TCN from satellite sensors showing smaller sensitivity to time signifies that the large temporal variability demonstrated in Pandora measurements in Seoul-SNU is attributable to the extreme spatial inhomogeneity of NO<sub>2</sub> concentration in the SMA incorporated with the boundary layer advection, especially during the afternoon (i.e. LEO satellite overpass time) (Judd et al. 2018), rather than the intrinsic variability of NO<sub>2</sub> due to its enrollment in various atmospheric photochemical reactions.

The number of temporally collocated measurements between Pandora and satellite sensors drastically increased as the averaging interval increased from  $\pm 1$  to  $\pm 5$  min, whereas the increasing trend became smaller between  $\pm 5$  and  $\pm 90$  min (Supplementary Figure S4). This implies that the standard observation schedule of PGN carries out the observation with sufficient frequency that the  $\pm 5$  min interval from the satellite overpass time generally assures the presence of collocated Pandora measurements (also shown in Figure 4a), while some occasional small clouds (i.e. small cumulus clouds during the daytime) in the FOV of Pandora can deteriorate the retrieval quality, hence, require a larger collocation interval. The number of collocated measurements between the satellite and Pandora (Figure 5 and Supplementary Figure S4) together with the uncertainty induced by the temporal variability of TCN in SMA (Figure 4b) means that the temporal collocation interval of  $\pm 5$  min seems adequate for Pandora-satellite TCN intercomparison in immensely polluted places, such as the SMA.

### 3.3. Spatial inhomogeneity of total column NO<sub>2</sub> and wind-based collocation

The wind-based method was applied for the collocation of TROPOMI and Pandora (Seoul-SNU) measurements to investigate the spatial distribution and transport pattern of NO<sub>2</sub> in the SMA as well as to comprehensively understand the discrepancy of TCN measured by TROPOMI and Pandora. Overall,  $\pm 5$  min from the coincident time (= TROPOMI overpass time  $\pm$  air mass travel time; see Section 2.3) was employed for the temporal collocation interval of Pandora measurements, an optimum temporal collocation interval in the SMA (see Section 3.2). The application of the wind-based method significantly increased the number of collocated measurements from 225 (conventional collocation) to 2874, while the

TROPOMI pixels located upwind and downwind of Pandora were separately accounted for in the analysis because they were expected to show different signatures. Furthermore, the TROPOMI TCN algorithm updates from v1.3 to v1.4 (modification of the FRESCO cloud algorithm) is known to have a significant influence on retrieved TCN (Eskes et al. 2020), and the data before and after the update have been separately considered accordingly.

Figures 6 and 7 show the scatterplot of TCN measured by TROPOMI and Pandora before (FRESCO-S) and after (FRESCO-wide) the FRESCO update, respectively. The figures are color indexed with possible factors that can influence the intercomparison results (i.e. the distance between the TROPOMI pixel and Pandora, travel time of an air mass, and cloud fraction of a TROPOMI pixel). The wind-based collocated TROPOMI and Pandora measurements exhibited comparable intercomparison scores as the conventional collocated measurements (shown in Figure 5a), but the correlation ( $R^2$ ) between the TROPOMI and Pandora measurements slightly decreased because of the complexity of the wind field near the urban surface. The negative bias of TROPOMI TCN compared to the coincident Pandora observations was pronounced, while the underestimation was generally smaller in the downwind pixels than the upwind pixels and after the FRESCO update than before. With the FRESCO-S algorithm (prior to the FRESCO update), the downwind pixels exhibited 30% lower TCN than the coincident Pandora, whereas the upwind pixels showed a 39% lower TCN. The FRESCO algorithm update from FRESCO-S to FRESCO-wide alleviated the magnitude of underestimation in both upwind and downwind pixels, but still 10% (downwind) and 32% (upwind) negative bias remained. Downwind pixels from the Seoul-SNU Pandora are believed to have been heavily affected by the massive vehicular NO<sub>2</sub> emissions from Seoul, whereas a substantial portion of the upwind pixels is yet to be affected by the direct emissions from an urban area of Seoul. Therefore, the difference between the downwind and upwind pixels signifies excessive NO<sub>2</sub> emissions, particularly in Seoul, compared to other cities in the SMA. Furthermore, Figure 6a, 6d, 7a, and 7d, and Table 2 show that the TROPOMI TCN measurements on the upwind side tend to underestimate more with increasing distance from the Seoul-SNU Pandora (Figures 6a and 7a), while a subtle opposite tendency is found in the downwind pixels (Figures 6d and 7d). This represents the sharp spatial gradient of NO<sub>2</sub>

concentrations around Seoul-SNU Pandora, while the emitted  $\text{NO}_2$  plume preserved its character during short-range transport ( $\sim 30$  km) through the downwind region. The travel time of an air mass, calculated by dividing the distance between Pandora and TROPOMI pixels by the wind speed, is not as critical as the distance itself in causing a negative bias (Figure 6b, 6e, 7b, and 7e). Therefore, the spatial inhomogeneity of the TCN and air mass transport are more compelling factors that influence the intercomparison of Pandora and TROPOMI in SMA than the inherent temporal variability of  $\text{NO}_2$  attributed to its photochemical reactivity. The intercomparison of Pandora and TROPOMI generally showed no explicit dependency on the cloud fraction of the TROPOMI pixel (Figure 6c, 6f, 7c, and 7f), but there

was a noticeable decrease where TROPOMI significantly underestimated TCN with CRF around 0.15 after the FRESKO update (Figure 7c and 7f). Moreover, some outliers showed abnormally high TROPOMI TCN compared to Pandora with a distinctively high cloud fraction (CRF > 0.3) after the FRESKO update (Figure 7f), suggesting the necessity of further comprehensive investigation of the AMF calculation in a hazy atmosphere, such as that in Seoul.

To further investigate the spatial variability of  $\text{NO}_2$  and its distribution in the SMA, the coincident Pandora and TROPOMI TCN measurements under different wind directions are presented in Figure 8 with the intercomparison scores. The average Pandora TCN varied significantly according to the wind direction; hence, the

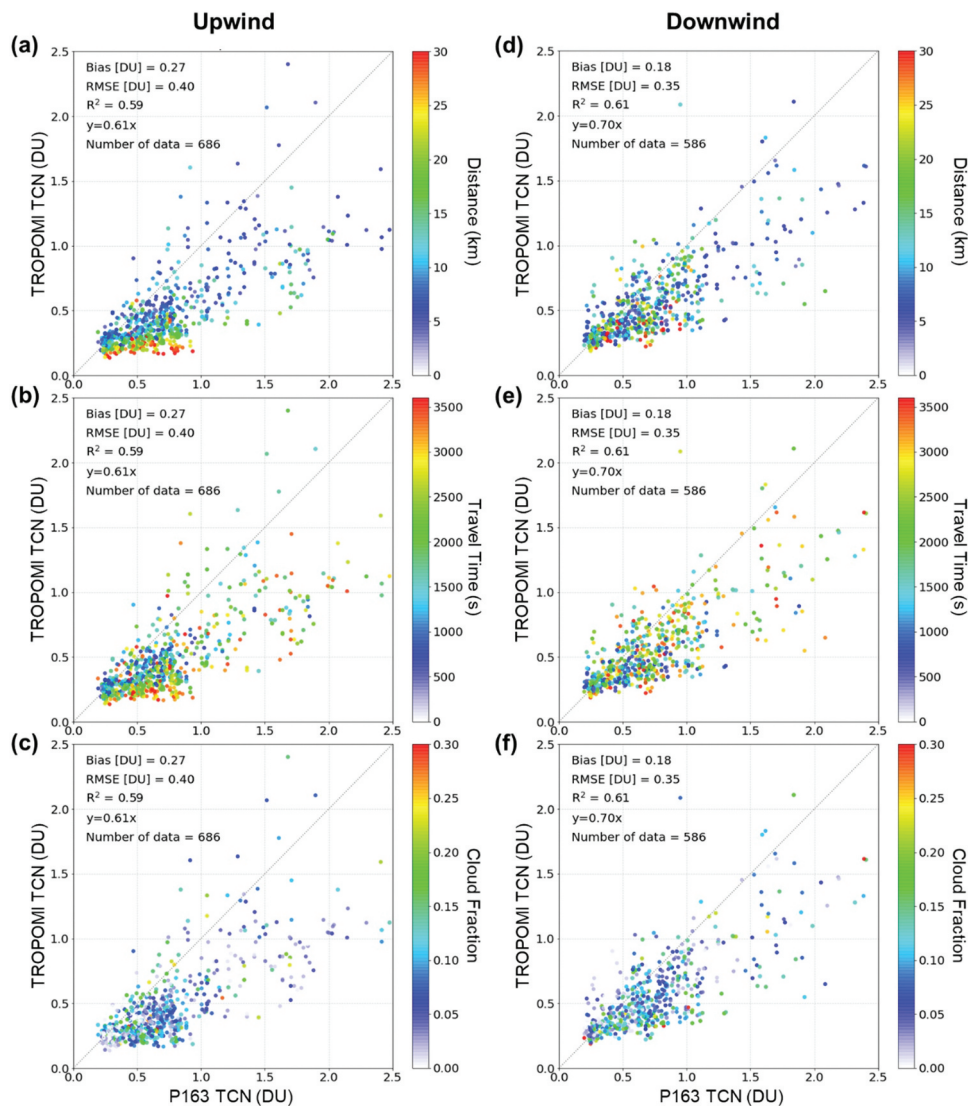


**Figure 6.** Comparison between TCN measured from P163 (Seoul-SNU) with coincident upwind (a, b, c) and downwind (d, e, f) TROPOMI pixels color-indexed with the TROPOMI pixel distance from Pandora (a, d), travel time of an air mass between TROPOMI pixel and Pandora (b, e), and cloud fraction of TROPOMI pixel (c, f) before the FRESKO cloud algorithm update (FRESKO-S).

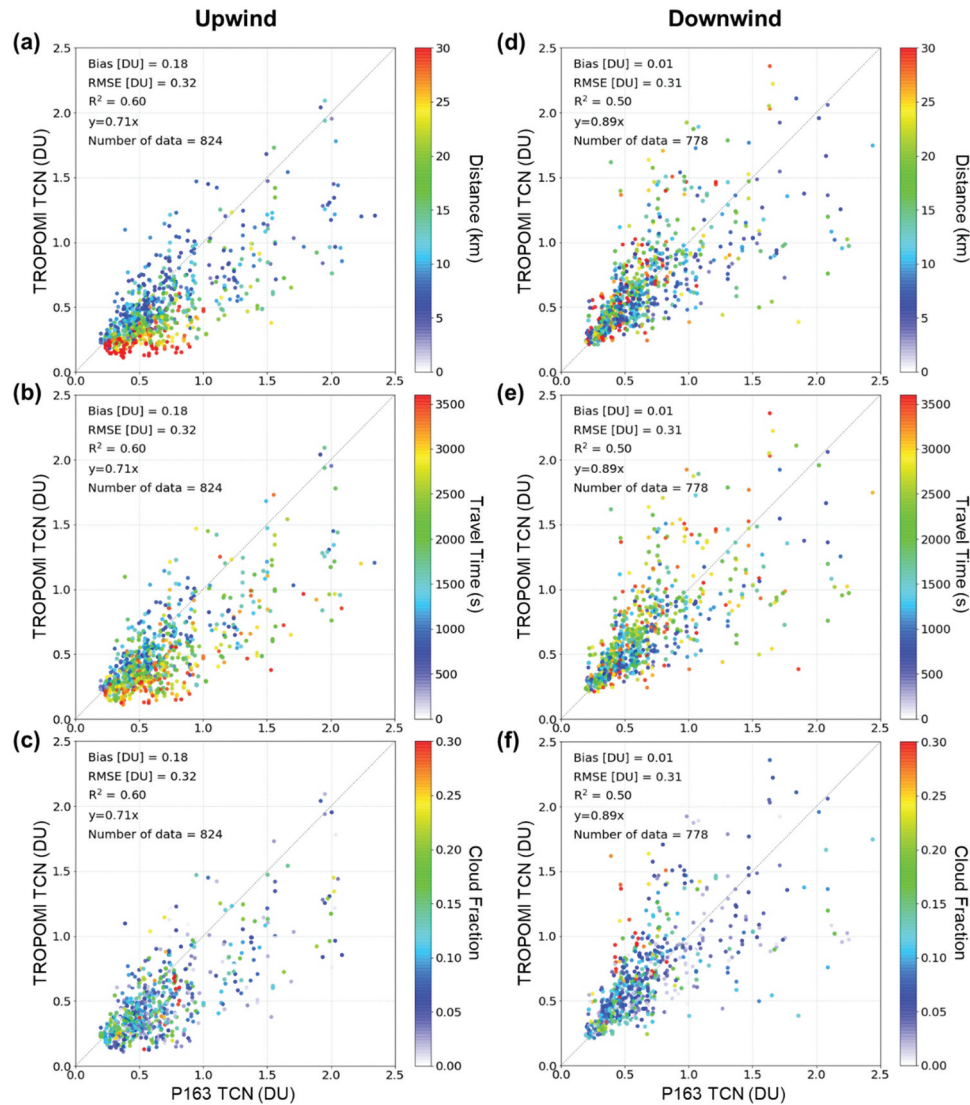


Figure 7. Same as Figure 6, but after the FRESCO cloud algorithm update (FRESCO-wide).

Table 2. Intercomparison scores of TCN from coincident Pandora and TROPOMI observations regarding the distance of TROPOMI pixels from the Pandora.

Scores	Before FRESCO update (FRESCO-S)						After FRESCO update (FRESCO-wide)					
	Upwind			Downwind			Upwind			Downwind		
	0–10	10–20	20–30	0–10	10–20	20–30	0–10	10–20	20–30	0–10	10–20	20–30
Distance (km)	0–10	10–20	20–30	0–10	10–20	20–30	0–10	10–20	20–30	0–10	10–20	20–30
Negative Bias (absolute, DU)	0.24	0.29	0.31	0.22	0.16	0.14	0.11	0.18	0.26	0.07	0.00	–0.05
Negative Bias (relative, %)	21.9	33.5	49.7	16.6	13.1	18.7	7.21	21.1	38.7	1.91	–8.30	–13.1
Regression slope	0.68	0.55	0.43	0.69	0.72	0.73	0.79	0.69	0.53	0.83	0.86	0.99
RMSE (DU)	0.40	0.41	0.36	0.38	0.36	0.24	0.31	0.31	0.33	0.28	0.34	0.33
R <sup>2</sup>	0.62	0.55	0.32	0.76	0.35	0.38	0.67	0.59	0.40	0.65	0.42	0.43
Counts	296	257	108	271	209	86	300	272	179	288	267	160

vicinity of Seoul-SNU Pandora can be classified as highly polluted (NE, SE, and W) and less polluted (E, SW, and NW) regions. The upwind TROPOMI pixels show almost consistent relative negative bias (33–41%, 0.07–0.37 DU)

to the coincident Pandora measurements in all wind directions, emphasizing that the NO<sub>2</sub> emissions are considerable throughout the SMA, even in the less-polluted regions. The downwind TROPOMI pixels, on the other

hand, showed smaller negative bias (13–33%, 0.01–0.19 DU) and even overestimated under the southwesterlies (6%, 0.09 DU), where the massive NO<sub>2</sub> emissions from downtown Seoul, located northeast of the Seoul-SNU Pandora site, are raising the actual TCN on the corresponding TROPOMI pixels. It is worth mentioning that the NW is the predominant surface wind direction over the SMA, which supports the regional NO<sub>2</sub> transport pattern discussed in Section 3.1 and shown in Figure 2b.

Figure 9 compares the Pandora and TROPOMI TCN, not only with respect to the wind direction, but also the distance between Pandora and TROPOMI pixels to obtain a two-dimensional spatial distribution pattern of NO<sub>x</sub> emissions. Downtown Seoul, with massive NO<sub>x</sub> emissions from vehicles, is located on the northeastern

side of Seoul-SNU (Supplementary Figure S1). Therefore, cases where TROPOMI showed a higher TCN than Pandora were found on the downwind side under southwesterlies over the downtown area (10–20 km from Seoul-SNU). The southwestern side of Seoul-SNU is generally not highly polluted, and is especially clean when the distance exceeds 15 km. Therefore, downwind pixels under northeasterlies generally showed a lower TCN when the distance from Pandora increased, whereas upwind pixels under southwesterlies underestimated TCN significantly when its distance from Seoul-SNU was greater than 15 km. The eastern side of Seoul-SNU is relatively clean, but some TROPOMI pixels with higher TCN than coincident Pandora measurements existed on the downwind side under westerlies, presumably due to

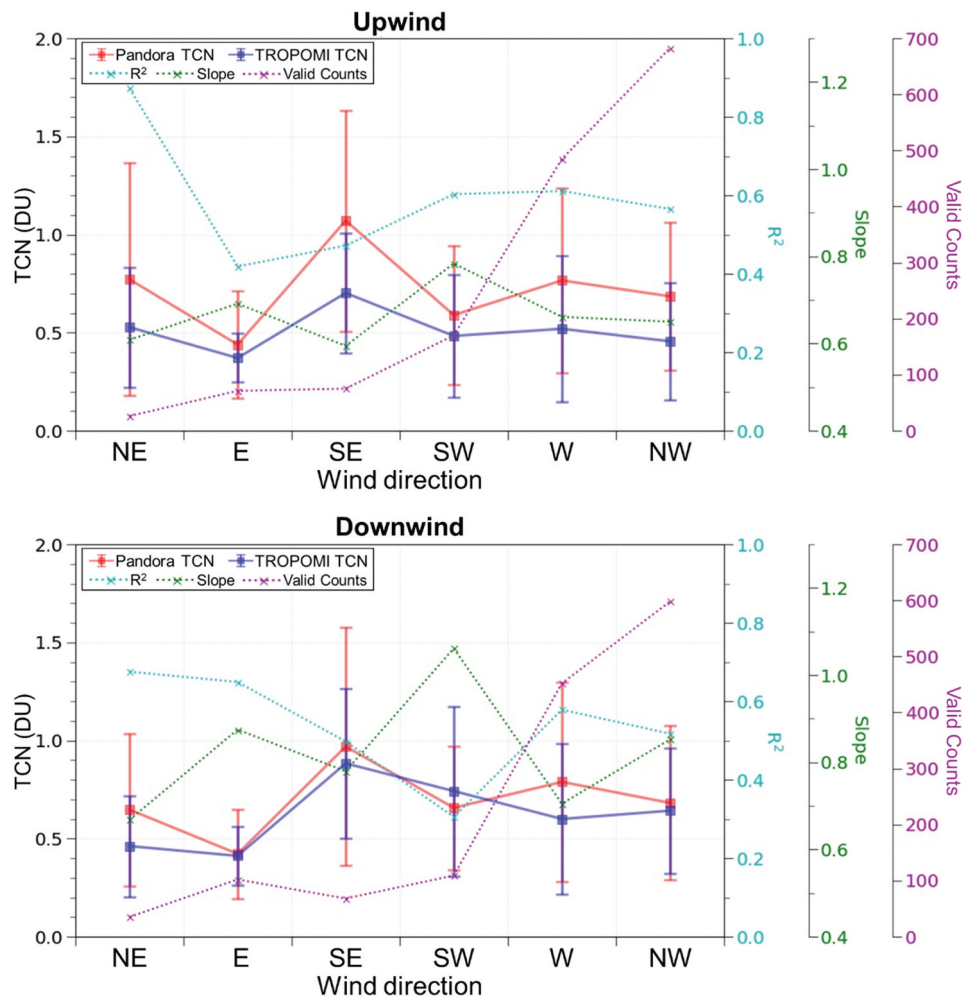


**Figure 8.** Intercomparison scores (mean and standard deviation of TCN, R<sup>2</sup>, zero-intercept slope, and valid counts) between TCN measured from collocated upwind (top) and downwind (bottom) TROPOMI pixels and Pandora (Seoul-SNU) according to the wind direction. The TCN measurements both before and after the FRESKO algorithm update are included.

the downtown area located on the eastern side (Gangnam, 10–15 km from Seoul-SNU; Supplementary Figure S1). The western side of Seoul-SNU is relatively polluted, where another megacity, Incheon, is located with concentrated industries and high-traffic loadings (ships, airplanes, and vehicles). In particular, the upwind TROPOMI pixels under westerlies showed a larger difference from Pandora TCN proportional to the distance between the TROPOMI pixel and Pandora at Seoul-SNU infers substantial  $\text{NO}_2$  emission along the transport pathway (western side of Seoul-SNU) influencing the air mass accumulatively during transport. Pandora TCN is excessively high under southeasterlies (highest among all wind directions) and has some positive bias of TROPOMI TCN in the distant downwind pixels (20–30 km away from Seoul-SNU) under northwesterlies. Major satellite cities (Suwon, Yongin, and Seongnam) and arterial roads (Supplementary Figure S1) are located on the southeast side of Seoul-SNU, but the observed  $\text{NO}_2$  concentrations were higher than those anticipated from the vehicle emissions in satellite cities with a much smaller population and traffic volume than downtown Seoul. Accordingly, there is a possibility of some unknown extra  $\text{NO}_x$  or its precursor sources approximately 20–30 km southeast of Seoul-SNU (i.e. semiconductor factories in Yongin/Giheong and Icheon [Lee, Ryu, and Moon 2012]). The northwestern side of Seoul-SNU is generally less polluted than the other sides, especially when the distance from the Pandora site exceeds 15 km, inferred from upwind TROPOMI pixels showing apparently low TCN under northwesterlies when the distance from Pandora becomes greater than 10–15 km. The boundary of Seoul on the northwestern side is approximately 15 km from Seoul-SNU, and the restricted area from then due to a hostile border with North Korea prohibits  $\text{NO}_x$  emissions.

The spatial distribution of TCN and inference of  $\text{NO}_x$  emission sources presented in Figures 8 and 9 are based on the TCN spatial distribution in the early afternoon (i.e. LEO satellite overpass time), but the  $\text{NO}_2$  plume might have been dispersed over the SMA from primary emission sources as the wind field varies since the morning (Judd et al. 2018). Therefore, the emission sources depicted in this study may not be precise, and incorporating more extended observations of Pandora and high-resolution satellite observations are required to ensure more accurate identification of the spatial distribution of major  $\text{NO}_x$  emission sources. Moreover, routine high-resolution

airborne measurements (i.e. GeoTASO and GCAS [Nowlan et al. 2016; Judd et al. 2020]) that can bridge between the satellite and ground-based Pandora and the multiple observations per day from GEO satellite sensor GEMS would complement the determination of the exact location and strength of point and areal emissions near the SMA.

#### 4. Summary and conclusions

This study investigated the spatiotemporal variability of TCN in the SMA using TROPOMI and Pandora (Seoul-SNU) measurements from October 2019 to May 2021. The TROPOMI observations showed that the average TCN in SMA (0.70; 0.83 DU in downtown Seoul) is comparable to the major Chinese polluted megacities (i.e. the BTH region and Shanghai). The Pandora measurements concordantly showed high TCN in Seoul and further revealed the diurnal variation pattern resembling a unimodal structure with consistently high TCN during the daytime (10–17 LST). The collocated Pandoras (P149 and P163) in Seoul-SNU showed satisfactory conformity ( $R^2 > 0.98$ ,  $\text{RMSE} < 0.06$  DU), whereas significant deterioration in autocorrelation scores of Pandora TCN with increasing time lag implied large temporal variability of TCN. In contrast, TCN measurements from satellite sensors and Pandora exhibited imperceptible degradation in intercomparison scores with temporal averaging interval enlargement. Therefore, the large temporal variability observed in Pandora TCN is attributable to the extreme spatial inhomogeneity of  $\text{NO}_2$  emissions in the SMA associated with advection in the boundary layer. The optimal temporal collocation range for Pandora TCN measurements with satellite observations was determined as  $\pm 5$  min, refraining from gaining uncertainty due to temporal variability of TCN ( $\text{RMSE} < 0.1$  DU) and considering the probability of the coincident Pandora measurements. Meanwhile, the TROPOMI was in the best agreement ( $0.72 < R^2 < 0.75$ , 26–29% negative bias) with conventionally collocated Pandora TCN measurements among the three satellite sensors (TROPOMI, OMI, and OMPS) because of its high spatial resolution.

The wind-based collocation method increased the number of coincident TCN measurements between TROPOMI and Pandora and further examined the spatial inhomogeneity of the TCN by incorporating the wind direction and distance between the TROPOMI pixels from Pandora. TROPOMI generally underestimates TCN compared to coincident Pandora measurements, with a

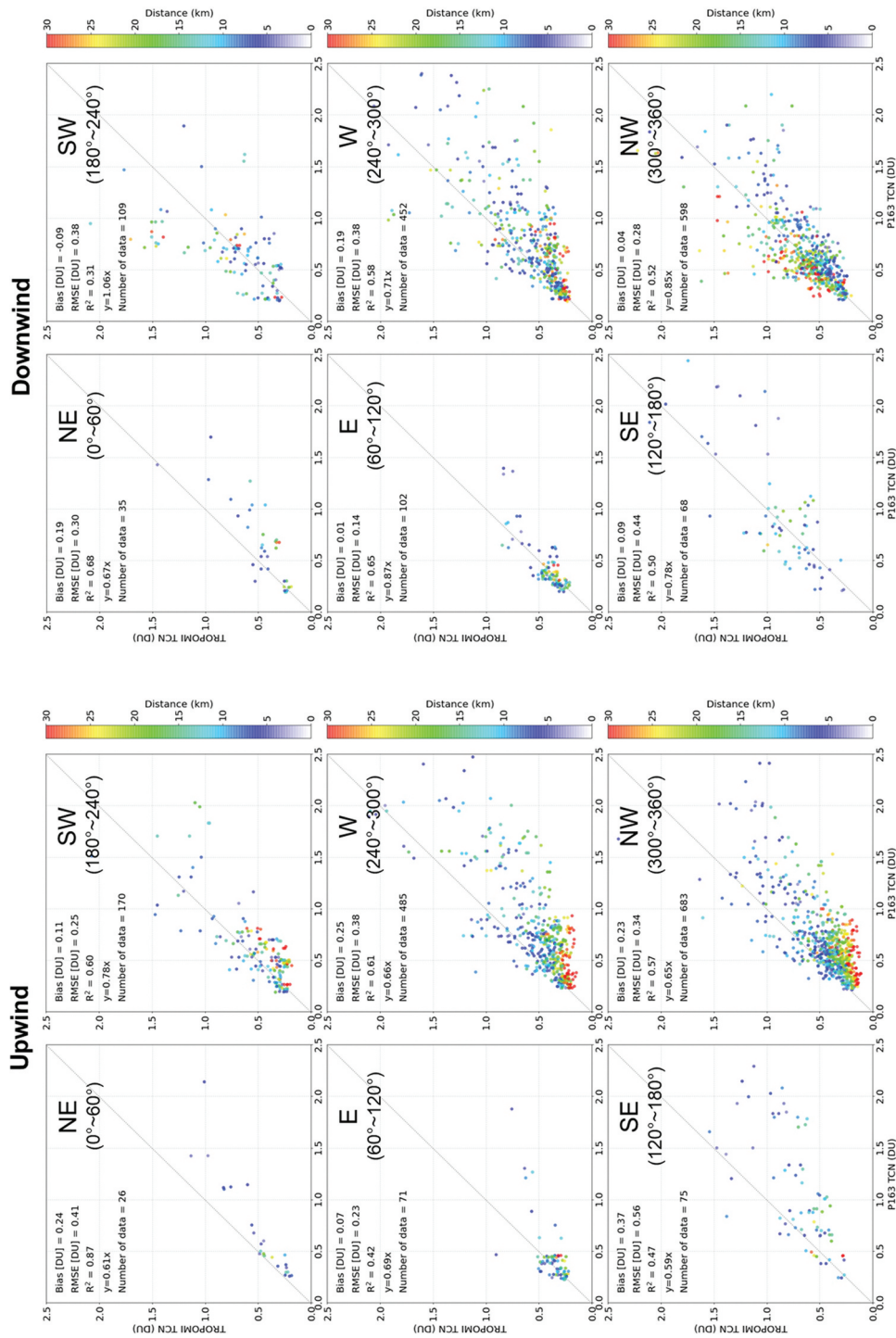


Figure 9. Comparison between TCNs measured from P163 (Seoul-SNU) with coincident upwind (left two columns) and downwind (right two columns) TROPOMI pixels according to the wind direction disregarding the FRESCO algorithm update.



smaller negative bias in downwind pixels (30%) compared to upwind pixels (39%). Moreover, the FRESCO algorithm update in the TROPOMI TCN retrievals reduced the negative bias, yielding 11% (downwind) and 29% (upwind) remaining bias. The distance between the TROPOMI pixel and Pandora (Seoul-SNU) was a critical factor determining the discrepancy of coincident TCN measured by Pandora and TROPOMI rather than the travel time of an air mass, consolidating the significance of the spatial inhomogeneity of NO<sub>2</sub> and advection. Furthermore, the wind-based method classified the relatively less-polluted (E, SW, NW) and more-polluted (NE, SE, W) regions referenced from the Pandora site (Seoul-SNU) and found some unexpectedly high emissions over the southeastern side, raising the possibility of unknown or excessive NO<sub>x</sub> (or its precursor) sources approximately 20–30 km away from Seoul-SNU.

Satellite-Pandora collocation based on the wind field demonstrated its utility and capability in an intercomparison of TCN measurements, even in a polluted urban environment. However, the upwind/downwind pixels should be used with meticulous investigations regarding the spatial distribution of emission sources and should strictly restrain the collocation distance when evaluating satellite TCN observations with ground-based Pandora observations. Quantification of the spatiotemporal variability of TCN and the guidelines presented in this study for a satellite-ground intercomparison can enlighten future environmental satellite validation strategies, whereas long-term observation of Pandora and temporally well-resolved wind field data can further improve the validation scores. Moreover, comprehensive error analysis of wind-based collocation methods regarding the respective spatiotemporal variability in various environments will be essential to be a bedrock strategy for the future validation of TCN retrieved from GEO satellites (i.e. GEMS, TEMPO, and Sentinel-4), which will enable a thorough and accurate understanding of the emission and transport of atmospheric NO<sub>2</sub>.

## Acknowledgements

This study was funded by the Fine Particle Research Initiative in East Asia Considering National Differences (FRIEND) through the National Research Foundation of Korea (NRF), funded by the Ministry of Science and ICT (Grant No.: 2020M3G1A1114615). Jin-Soo Park and Hyun-Jae Kim were supported by NIER research grants (NIER-2021-01-01-109). The PGN is a bilateral project supported with funding from NASA and ESA. We thank the

PI(s), support staff, and funding for establishing and maintaining the Busan site of the PGN and KORUS-AQ team operating and processing the data used in this investigation.

## Author contributions

Jong-Uk Park: Conceptualization, Formal analysis, Visualization, Writing - original draft. Jin-Soo Park and Hyun-Jae Kim: Data curation, Writing - review & editing. Daniel Santana Diaz and Manuel Gebetsberger: Data curation. Moritz Müller: Data curation, Writing - review & editing. Lena Shalaby: Data curation. Martin Tiefengraber: Data curation, Writing - review & editing. Sang-Seo Park: Methodology, Writing - review & editing. Chang-Keun Song: Data curation, Writing - review, and editing. Sang-Woo Kim: Conceptualization, Writing - review and editing.

## Data and codes availability statement

The data and codes that support the findings of this study are available at <https://doi.org/10.7910/DVN/1Y0Z06>

## Disclosure statement

The authors declare that they have no known competing financial interests or personal relationships that could have appeared to influence the work reported in this paper.

## Funding

This work was supported by the National Institute of Environmental Research [NIER-2021-01-01-109]; National Institute of Environmental Research [NIER-2021-01-01-109]; National Research Foundation of Korea [2020M3G1A1114615].

## ORCID

Jong-Uk Park  <http://orcid.org/0000-0001-8209-6031>

Chang-Keun Song  <http://orcid.org/0000-0002-8987-2176>

Sang-Woo Kim  <http://orcid.org/0000-0003-1279-8331>

## References

- Beirle, S., C. Borger, S. Dörner, A. Li, Z. Hu, F. Liu, Y. Wang, and T. Wagner. 2019. "Pinpointing Nitrogen Oxide Emissions from Space." *Science Advances* 5 (11): 1–7. doi:10.1126/sciadv.aax9800.
- Beirle, S., H. Huntrieser, and T. Wagner. 2010. "Direct Satellite Observation of Lightning-Produced NO<sub>x</sub>." *Atmospheric Chemistry and Physics* 10 (22): 10965–10986. doi:10.5194/acp-10-10965-2010.

- Beirle, S., K. F. Boersma, U. Platt, M. G. Lawrence, and T. Wagner. 2011. "Megacity Emissions and Lifetimes of Nitrogen Oxides Probed from Space." *Science* 333 (6050): 1737–1739. doi:10.1126/science.1207824.
- Belmonte Rivas, M., P. Veefkind, F. Boersma, P. Levelt, H. Eskes, and J. Gille. 2014. "Intercomparison of daytime Stratospheric NO<sub>2</sub> Satellite Retrievals and Model Simulations." *Atmospheric Measurement Techniques* 7 (7): 2203–2225. doi:10.5194/amt-7-2203-2014.
- Boersma, K. F., D. J. Jacob, M. Trainic, Y. Rudich, I. deSmedt, R. Dirksen, and H. J. Eskes. 2009. "Validation of Urban NO<sub>2</sub> Concentrations and Their Diurnal and Seasonal Variations Observed from the SCIAMACHY and OMI Sensors Using in Situ Surface Measurements in Israeli Cities." *Atmospheric Chemistry and Physics* 9 (12): 3867–3879. doi:10.5194/acp-9-3867-2009.
- Boersma, K. F., H. J. Eskes, A. Richter, I. de Smedt, A. Lorente, S. Beirle, J. H. G. M. van Geffen *et al.* 2018. "Improving Algorithms and Uncertainty Estimates for Satellite NO<sub>2</sub> Retrievals: Results from the Quality Assurance for the Essential Climate Variables (QA4ECV) Project." *Atmospheric Measurement Techniques* 11 (12): 6651–6678. doi:10.5194/amt-11-6651-2018.
- Boersma, K. F., H. J. Eskes, R. J. Dirksen, J. P. Veefkind, P. Stammes, and V. Huijnen. 2011. "An Improved Tropospheric NO<sub>2</sub> Column Retrieval Algorithm for the Ozone Monitoring Instrument." *Atmospheric Measurement Techniques* 4 (9): 1905–1928. doi:10.5194/amt-4-1905-2011.
- Bovensmann, H., J. P. Burrows, M. Buchwitz, J. Frerick, S. Noël, V. V. Rozanov, K. V. Chance, and A. P. H. Goede. 1999. "SCIAMACHY: Mission Objectives and Measurement Modes." *Journal of the Atmospheric Sciences* 56 (2): 127–150. doi:10.1175/1520-0469(1999)056<0127:SMOAMM>2.0.CO;2.
- Broccardo, S., K.-P. Hueue, D. Walter, C. Meyer, A. Kokhanovsky, R. van der A, S. Piketh, K. Langerman, and U. Platt. 2018. "Intra-Pixel Variability in Satellite Tropospheric NO<sub>2</sub> Column Densities Derived from Simultaneous Space-Borne and Airborne Observations over the South African Highveld." *Atmospheric Measurement Techniques* 11 (5): 2797–2819. doi:10.5194/amt-11-2797-2018.
- Burrows, J. P., M. Buchwitz, V. Rozanov, M. Weber, A. Richter, A. Ladstätter-Weißenmayer, and M. Eisinger. 1997. "The Global Ozone Monitoring Experiment (GOME): Mission, Instrument Concept, and First Scientific Results." European Space Agency, (Special Publication) ESA SP, no. 414 PART 2: 585–590.
- Bytnerowicz, A., K. Omasa, and E. Paoletti. 2007. "Integrated Effects of Air Pollution and Climate Change on Forests: A Northern Hemisphere Perspective." *Environmental Pollution* 147 (3): 438–445. doi:10.1016/j.envpol.2006.08.028.
- Cede, A., J. Herman, A. Richter, N. Krotkov, and J. Burrows. 2006. "Measurements of Nitrogen Dioxide Total Column Amounts Using a Brewer Double Spectrophotometer in Direct Sun Mode." *Journal of Geophysical Research Atmospheres* 111 (D5): 1–12. doi:10.1029/2005JD006585.
- Celarié, E. A., E. J. Brinksma, J. F. Gleason, J. P. Veefkind, A. Cede, J. R. Herman, D. Ionov *et al.* 2008. "Validation of Ozone Monitoring Instrument Nitrogen Dioxide Columns." *Journal of Geophysical Research* 113 (D15): D15S15. doi:10.1029/2007JD008908.
- Compernelle, S., A. Argyrouli, R. Lutz, M. Sneep, J.-C. Lambert, A. M. Fjæraa, D. Hubert *et al.* 2021. "Validation of the Sentinel-5 Precursor TROPOMI Cloud Data with Cloudnet, Aura OMI O<sub>2</sub>–O<sub>2</sub>, MODIS, and Suomi-NPP VIIRS." *Atmospheric Measurement Techniques* 14 (3): 2451–2476. doi:10.5194/amt-14-2451-2021.
- Crawford, J. H., J.-Y. Ahn, J. Al-Saadi, L. K. Limseok Chang, J. K. Emmons, J. Kim, G. Lee *et al.* 2021. "The Korea–United States Air Quality (KORUS-AQ) Field Study." *Elementa: Science of the Anthropocene* 9 (1): 1–27. doi:10.1525/elementa.2020.00163.
- ESA, KNMI. 2019. "Sentinel-5P TROPOMI Tropospheric NO<sub>2</sub> 1-Orbit L2 5.5km x 3.5km". Greenbelt, MD, USA, Goddard Earth Sciences Data and Information Services Center (GESDISC). Accessed 1 June 2021. Copernicus Sentinel data. doi:10.5270/S5P-s4ljg54
- Eskes, H. J., and K.-U. Eichmann. 2020. "S5P Mission Performance Centre Nitrogen Dioxide [L2\_NO2\_] Readme." Issue 1.6 (S5P-MPC-KNMI-PRF-NO2).
- Eskes, H., J. van Geffen, K. F. Boersma, K.-U. Eichmann, A. Apituley, M. Pedernana, M. Sneep, J. P. Veefkind, and D. Loyola. 2020. "Sentinel-5 precursor/TROPOMI Level 2 Product User Manual Nitrogen Dioxide." V.4.0.0 (S5P-KNMI-L2-0021-MA).
- Flynn, C. M., K. E. Pickering, J. H. Crawford, L. Lamsal, N. Krotkov, J. Herman, A. Weinheimer *et al.* 2014. "Relationship between Column-Density and Surface Mixing Ratio: Statistical Analysis of O<sub>3</sub> and NO<sub>2</sub> Data from the July 2011 Maryland DISCOVER-AQ Mission." *Atmospheric Environment* 92:429–441. doi:10.1016/j.atmosenv.2014.04.041. Elsevier Ltd.
- Gaffin, J. M., M. Hauptman, C. R. Petty, W. J. Sheehan, P. S. Lai, J. M. Wolfson, D. R. Gold, B. A. Coull, P. Koutrakis, and W. Phipatanakul. 2018. "Nitrogen Dioxide Exposure in School Classrooms of Inner-City Children with Asthma." *Journal of Allergy and Clinical Immunology* 141 (6): 2249–2255.e2. doi:10.1016/j.jaci.2017.08.028.
- Gil, M., M. Yela, L. N. Gunn, A. Richter, I. Alonso, M. P. Chipperfield, E. Cuevas *et al.* 2008. "NO<sub>2</sub> Climatology in the Northern Subtropical Region: Diurnal, Seasonal and Interannual Variability." *Atmospheric Chemistry and Physics* 8 (6): 1635–1648. doi:10.5194/acp-8-1635-2008.
- Goldberg, D. L., Z. Lu, D. G. Streets, B. de foy, D. Griffin, C. A. McLinden, L. N. Lamsal, N. A. Krotkov, and H. Eskes. 2019. "Enhanced Capabilities of TROPOMI NO<sub>2</sub>: Estimating NO<sub>x</sub> from North American Cities and Power Plants." *Environmental Science and Technology* 53 (21): 12594–12601. doi:10.1021/acs.est.9b04488.
- Griffin, D., X. Zhao, C. A. McLinden, F. Boersma, A. Bourassa, E. Dammers, D. Degenstein *et al.* 2019. "High-Resolution Mapping of Nitrogen Dioxide with TROPOMI: First Results and Validation over the Canadian Oil Sands." *Geophysical Research Letters* 46 (2): 1049–1060. doi:10.1029/2018GL081095.
- Herman, J., A. Cede, E. Spinei, G. Mount, M. Tzortziou, and N. Abuhassan. 2009. "NO<sub>2</sub> Column Amounts from Ground-based Pandora and MFDOAS Spectrometers Using the Direct-sun

- DOAS Technique: Intercomparisons and Application to OMI Validation." *Journal of Geophysical Research Atmospheres* 114 (D13): 1–20. doi:10.1029/2009jd011848.
- Herman, J., E. Spinei, A. Fried, J. Kim, J. Kim, W. Kim, A. Cede, N. Abuhassan, and M. Segal-Rozenhaimer. 2018. "NO<sub>2</sub> and HCHO Measurements in Korea from 2012 to 2016 from Pandora Spectrometer Instruments Compared with OMI Retrievals and with Aircraft Measurements during the KORUS-AQ Campaign." *Atmospheric Measurement Techniques* 11 (8): 4583–4603. doi:10.5194/amt-11-4583-2018.
- Herman, J., N. Abuhassan, J. Kim, J. Kim, M. Dubey, M. Raponi, and M. Tzortziou. 2019. "Underestimation of Column NO<sub>2</sub> Amounts from the OMI Satellite Compared to Diurnally Varying Ground-Based Retrievals from Multiple PANDORA Spectrometer Instruments." *Atmospheric Measurement Techniques* 12 (10): 5593–5612. doi:10.5194/amt-12-5593-2019.
- Herman, J., R. Evans, A. Cede, N. Abuhassan, I. Petropavlovskikh, and G. McConville. 2015. "Comparison of Ozone Retrievals from the Pandora Spectrometer System and Dobson Spectrophotometer in Boulder, Colorado." *Atmospheric Measurement Techniques* 8 (8): 3407–3418. doi:10.5194/amt-8-3407-2015.
- Hersbach, H., B. Bell, P. Berrisford, G. Biavati, A. Horányi, J. Muñoz Sabater, J. Nicolas *et al.* 2018. "ERA5 Hourly Data on Pressure Levels from 1979 to Present." Copernicus Climate Change Service (C3S) Climate Data Store (CDS). (Accessed on 1 June 2021).
- Hersbach, H., B. Bell, P. Berrisford, S. Hirahara, A. Horányi, J. Muñoz-Sabater, J. Nicolas *et al.* 2020. "The ERA5 Global Reanalysis." *Quarterly Journal of the Royal Meteorological Society* 146 (730): 1999–2049. doi:10.1002/qj.3803.
- Ialongo, I., H. Virta, H. Eskes, J. Hovila, and J. Douros. 2020. "Comparison of TROPOMI/Sentinel-5 Precursor NO<sub>2</sub> Observations with Ground-Based Measurements in Helsinki." *Atmospheric Measurement Techniques* 13 (1): 205–218. doi:10.5194/amt-13-205-2020.
- Ialongo, I., J. Herman, N. Krotkov, L. Lamsal, K. F. Boersma, J. Hovila, and J. Tamminen. 2016. "Comparison of OMI NO<sub>2</sub> Observations and Their Seasonal and Weekly Cycles with Ground-Based Measurements in Helsinki." *Atmospheric Measurement Techniques* 9 (10): 5203–5212. doi:10.5194/amt-9-5203-2016.
- Jacob, D. J. 2000. "Heterogeneous Chemistry and Tropospheric Ozone." *Atmospheric Environment* 34 (12–14): 2131–2159. doi:10.1016/S1352-2310(99)00462-8.
- Jaeglé, L., L. Steinberger, R. V. Martin, and K. Chance. 2005. "Global Partitioning of NO<sub>x</sub> Sources Using Satellite Observations: Relative Roles of Fossil Fuel Combustion, Biomass Burning and Soil Emissions." *Faraday Discussions* 130 (x): 407–423. doi:10.1039/b502128f.
- Jeong, U., and H. Hong. 2021. "Assessment of Tropospheric Concentrations of NO<sub>2</sub> from the TROPOMI/Sentinel-5 Precursor for the Estimation of Long-Term Exposure to Surface NO<sub>2</sub> over South Korea." *Remote Sensing* 13 (10): 1877. doi:10.3390/rs13101877.
- Jo, S., Y.-J. Kim, K. W. Park, Y. S. Hwang, S. H. Lee, B. J. Kim, and S. J. Chung. 2021. "Association of NO<sub>2</sub> and Other Air Pollution Exposures with the Risk of Parkinson Disease." *JAMA Neurology* 78 (8): 1–9. doi:10.1001/jama.2021.2135.
- Jonson, J. E., J. Borken-Kleefeld, D. Simpson, A. Nyíri, M. Posch, and C. Heyes. 2017. "Impact of Excess NO<sub>x</sub> Emissions from Diesel Cars on Air Quality, Public Health and Eutrophication in Europe." *Environmental Research Letters* 12 (9): 9. doi:10.1088/1748-9326/aa8850.
- Judd, L. M., J. A. Al-Saadi, J. J. Szykman, L. C. Valin, S. J. Janz, M. G. Kowalewski, H. J. Eskes *et al.* 2020. "Evaluating Sentinel-5P TROPOMI Tropospheric NO<sub>2</sub> Column Densities with Airborne and Pandora Spectrometers near New York City and Long Island Sound." *Atmospheric Measurement Techniques* 13 (11): 6113–6140. doi:10.5194/amt-13-6113-2020.
- Judd, L. M., J. A. Al-Saadi, L. C. Valin, R. Bradley Pierce, K. Yang, S. J. Janz, M. G. Kowalewski *et al.* 2018. "The Dawn of Geostationary Air Quality Monitoring: Case Studies from Seoul and Los Angeles." *Frontiers in Environmental Science* 6 : 85. doi:10.3389/fenvs.2018.00085.
- Judd, L. M., J. A. Al-Saadi, S. J. Janz, M. G. Kowalewski, R. B. Pierce, J. J. Szykman, L. C. Valin *et al.* 2019. "Evaluating the Impact of Spatial Resolution on Tropospheric NO<sub>2</sub> Column Comparisons within Urban Areas Using High-Resolution Airborne Data." *Atmospheric Measurement Techniques* 12 (11): 6091–6111. doi:10.5194/amt-12-6091-2019.
- Kampa, M., and E. Castanas. 2008. "Human Health Effects of Air Pollution." *Environmental Pollution* 151 (2): 362–367. doi:10.1016/j.envpol.2007.06.012.
- Kim, H. C., P. Lee, L. Judd, L. Pan, and B. Lefer. 2016. "OMI NO<sub>2</sub> Column Densities over North American Urban Cities: The Effect of Satellite Footprint Resolution." *Geoscientific Model Development* 9 (3): 1111–1123. doi:10.5194/gmd-9-1111-2016.
- Kim, H. C., S. Kim, S. H. Lee, B. U. Kim, and P. Lee. 2020a. "Fine-Scale Columnar and Surface NO<sub>x</sub> Concentrations over South Korea: Comparison of Surface Monitors, TROPOMI, CMAQ and CAPS Inventory." *Atmosphere* 11 (1): 101. doi:10.3390/ATMOS11010101.
- Kim, J., U. Jeong, M. H. Ahn, J. H. Kim, R. J. Park, H. Lee, C. H. Song *et al.* 2020b. "New Era of Air Quality Monitoring from Space: Geostationary Environment Monitoring Spectrometer (GEMS)." *Bulletin of the American Meteorological Society* 101 (1): E1–E22. doi:10.1175/BAMS-D-18-0013.1.
- Kim, M.-H., H. Yeo, S. Park, D.-H. Park, A. Omar, T. Nishizawa, A. Shimizu, and S.-W. Kim. 2021. "Assessing CALIOP-Derived Planetary Boundary Layer Height Using Ground-Based Lidar." *Remote Sensing* 13 (8): 1496. doi:10.3390/rs13081496.
- Kim, N. K., Y. P. Kim, Y. Morino, J.-i. Kurokawa, and T. Ohara. 2013. "Verification of NO<sub>x</sub> Emission Inventory over South Korea Using Sectoral Activity Data and Satellite Observation of NO<sub>2</sub> Vertical Column Densities." *Atmospheric Environment* 77 : 496–508. doi:10.1016/j.atmosenv.2013.05.042. .

- Kleipool, Q. L., M. R. Dobber, J. F. de Haan, and P. F. Levelt. 2008. "Earth Surface Reflectance Climatology from 3 Years of OMI Data." *Journal of Geophysical Research Atmospheres* 113 (D18): 1–22. doi:10.1029/2008JD010290.
- Kleipool, Q., A. Ludewig, L. Babić, R. Bartstra, R. Braak, W. Dierssen, P.-J. Dewitte *et al.* 2018. "Pre-Launch Calibration Results of the TROPOMI Payload on-Board the Sentinel-5 Precursor Satellite." *Atmospheric Measurement Techniques* 11 (12): 6439–6479. doi:10.5194/amt-11-6439-2018.
- Laj, P., A. Bigi, C. Rose, E. Andrews, C. Lund Myhre, M. Collaud Coen, A. Wiedensohler *et al.* 2020. "A Global Analysis of Climate-Relevant Aerosol Properties Retrieved from the Network of GAW near-Surface Observatories." *Atmospheric Measurement Techniques* 13 4353–4392. doi:10.5194/amt-13-4353-2020.
- Lamsal, L. N., N. A. Krotkov, S. V. Marchenko, J. Joiner, L. Oman, A. Vasilkov, B. Fisher *et al.* 2020. "OMI/Aura NO<sub>2</sub> Tropospheric, Stratospheric & Total Columns MINDS 1-Orbit L2 Swath 13 Km X 24 Km." NASA Goddard Space Flight Center, Goddard Earth Sciences Data and Information Services Center (GES DISC), Accessed: [1 June 2021], doi: 10.5067/MEASURES/MINDS/DATA201.
- Langford, A. O., R. Schofield, J. S. Daniel, R. W. Portmann, M. L. Melamed, H. L. Miller, E. G. Dutton, and S. Solomon. 2007. "On the Variability of the Ring Effect in the near Ultraviolet: Understanding the Role of Aerosols and Multiple Scattering." *Atmospheric Chemistry and Physics* 7 (3): 575–586. doi:10.5194/acp-7-575-2007.
- Lee, S.-J., I.-S. Ryu, and S.-H. Moon. 2012. "N<sub>2</sub>O Emission and Reduction in the Electronics Manufacturing Industries." *Greenhouse Gases: Science and Technology* 2 (5): 380–385. doi:10.1002/ghg.1301.
- Levelt, P. F., G. H. J. van den Oord, M. R. Dobber, A. Malkki, H. Visser, J. de Vries, P. Stammes, J. O. V. Lundell, and H. Saari. 2006. "The Ozone Monitoring Instrument." *IEEE Transactions on Geoscience and Remote Sensing* 44 (5): 1093–1100. doi:10.1109/TGRS.2006.872333.
- Levelt, P. F., J. Joiner, J. Tamminen, J. P. Veefkind, P. K. Bhartia, D. C. Stein Zweers, B. N. Duncan *et al.* 2018. "The Ozone Monitoring Instrument: Overview of 14 Years in Space." *Atmospheric Chemistry and Physics* 18 (8): 5699–5745. doi:10.5194/acp-18-5699-2018.
- Liu, F., S. Beirle, Q. Zhang, S. Dörner, K. He, and T. Wagner. 2016. "NO<sub>x</sub> Lifetimes and Emissions of Cities and Power Plants in Polluted Background Estimated by Satellite Observations." *Atmospheric Chemistry and Physics* 16 (8): 5283–5298. doi:10.5194/acp-16-5283-2016.
- Liu, M., J. Lin, H. Kong, K. F. Boersma, H. Eskes, Y. Kanaya, Q. He *et al.* 2020. "A New TROPOMI Product for Tropospheric NO<sub>2</sub> Columns over East Asia with Explicit Aerosol Corrections." *Atmospheric Measurement Techniques* 13 (8): 4247–4259. doi:10.5194/amt-13-4247-2020.
- Liu, S., P. Valks, G. Pinardi, I. De Smedt, H. Yu, S. Beirle, and A. Richter. 2019. "An Improved Total and Tropospheric NO<sub>2</sub> Column Retrieval for GOME-2." *Atmospheric Measurement Techniques* 12 (2): 1029–1057. doi:10.5194/amt-12-1029-2019.
- Martin, R. V., D. J. Jacob, K. Chance, T. P. Kurosu, P. I. Palmer, and M. J. Evans. 2003. "Global Inventory of Nitrogen Oxide Emissions Constrained by Space-based Observations of NO<sub>2</sub> Columns." *Journal of Geophysical Research: Atmospheres* 108 (D17): 1–12. doi:10.1029/2003jd003453.
- Munro, R., R. Lang, D. Klaes, G. Poli, C. Retscher, R. Lindstrot, R. Huckle *et al.* 2016. "The GOME-2 Instrument on the Metop Series of Satellites: Instrument Design, Calibration, and Level 1 Data Processing - an Overview." *Atmospheric Measurement Techniques* 9 (3): 1279–1301. doi:10.5194/amt-9-1279-2016.
- Nowlan, C. R., X. Liu, S. J. Janz, M. G. Kowalewski, K. Chance, M. B. Follette-Cook, A. Fried *et al.* 2018. "Nitrogen Dioxide and Formaldehyde Measurements from the GEOstationary Coastal and Air Pollution Events (GEO-CAPE) Airborne Simulator over Houston, Texas." *Atmospheric Measurement Techniques Discussions* 2 (2): 1–36. doi:10.5194/amt-2018-156.
- Nowlan, C. R., X. Liu, J. W. Leitch, K. Chance, G. G. Abad, C. Liu, P. Zogman *et al.* 2016. "Nitrogen Dioxide Observations from the Geostationary Trace Gas and Aerosol Sensor Optimization (Geotaso) Airborne Instrument: Retrieval Algorithm and Measurements during DISCOVER-AQ Texas 2013." *Atmospheric Measurement Techniques* 9 (6): 2647–2668. doi:10.5194/amt-9-2647-2016.
- Park, S. S., S. W. Kim, C. K. Song, J. U. Park, and K. H. Bae. 2020. "Spatio-Temporal Variability of Aerosol Optical Depth, Total Ozone and NO<sub>2</sub> over East Asia: Strategy for the Validation to the GEMS Scientific Products." *Remote Sensing* 12 (14): 14. doi:10.3390/rs12142256.
- Park, S., S.-W. Kim, M.-S. Park, and C.-K. Song. 2018. "Measurement of Planetary Boundary Layer Winds with Scanning Doppler Lidar." *Remote Sensing* 10 (8): 1261. doi:10.3390/rs10081261.
- Platt, U., and J. Stutz. 2008. *Differential Optical Absorption Spectroscopy: Principles and Applications*. Berlin, Germany: Springer-Verlag.
- Richards, L. W. 1983. "Comments on the Oxidation of NO<sub>2</sub> to Nitrate—day and Night." *Atmospheric Environment* (1967) 17 (2): 397–402. doi:10.1016/0004-6981(83)90057-4.
- Schenkeveld, V. M. E., G. Jaross, S. Marchenko, D. Haffner, Q. L. Kleipool, N. C. Rozemeijer, J. P. Veefkind, and P. F. Levelt. 2017. "In-Flight Performance of the Ozone Monitoring Instrument." *Atmospheric Measurement Techniques* 10 (5): 1957–1986. doi:10.5194/amt-10-1957-2017.
- Seftor, C. J., G. Jaross, M. Kowitt, M. Haken, J. Li, and L. E. Flynn. 2014. "Postlaunch Performance of the Suomi National Polar-orbiting Partnership Ozone Mapping and Profiler Suite (OMPS) Nadir Sensors." *Journal of Geophysical Research: Atmospheres* 119 (7): 4413–4428. doi:10.1002/2013JD020472.
- Serduchenko, A., V. Gorshchev, M. Weber, W. Chehade, and J. P. Burrows. 2014. "High Spectral Resolution Ozone Absorption Cross-Sections - Part 2: Temperature Dependence." *Atmospheric Measurement Techniques* 7 (2): 625–636. doi:10.5194/amt-7-625-2014.
- Sillman, S. 1999. "The Relation between Ozone, NO<sub>x</sub> and Hydrocarbons in Urban and Polluted Rural Environments." *Atmospheric Environment* 33 (12): 1821–1845. doi:10.1016/S1352-2310(98)00345-8.

- Solomon, S., J. M. Russell III, and L. L. Gordley. 1986. "Observations of the Diurnal Variation of Nitrogen Dioxide in the Stratosphere." *Journal of Geophysical Research* 91 (D5): 5455–5464. doi:10.1029/JD091iD05p05455.
- Tilstra, L. G., O. N. E. Tuinder, P. Wang, and P. Stammes. 2017. "Surface Reflectivity Climatologies from UV to NIR Determined From Earth Observations by GOME-2 and SCIAMACHY." *Journal of Geophysical Research* 122 (7): 4084–4111. doi:10.1002/2016JD025940.
- Tzortziou, M., J. R. Herman, C. P. Alexander Cede, N. A. Loughner, and S. Naik. 2015. "Spatial and Temporal Variability of Ozone and Nitrogen Dioxide over a Major Urban Estuarine Ecosystem." *Journal of Atmospheric Chemistry* 72 (3–4): 287–309. doi:10.1007/s10874-013-9255-8.
- Valin, L. C., A. R. Russell, E. J. Bucsela, J. P. Veefkind, and R. C. Cohen. 2011a. "Observation of Slant Column NO<sub>2</sub> Using the Super-Zoom Mode of AURA-OMI." *Atmospheric Measurement Techniques* 4 (9): 1929–1935. doi:10.5194/amt-4-1929-2011.
- Valin, L. C., A. R. Russell, R. C. Hudman, and R. C. Cohen. 2011b. "Effects of Model Resolution on the Interpretation of Satellite NO<sub>2</sub> Observations." *Atmospheric Chemistry and Physics* 11 (22): 11647–11655. doi:10.5194/acp-11-11647-2011.
- van der A, R. J., H. J. Eskes, K. F. Boersma, T. P. C. van Noije, M. van Roozendael, I. De Smedt, D. H. M. U. Peters, and E. W. Meijer. 2008. "Trends, Seasonal Variability and Dominant NO<sub>x</sub> Source Derived from a Ten Year Record of NO<sub>2</sub> Measured from Space." *Journal of Geophysical Research Atmospheres* 113 (D17): 1–12. doi:10.1029/2003JD003453.
- van Geffen, J. H. G. M., H. J. Eskes, K. F. Boersma, J. D. Maasackers, and J. P. Veefkind. 2019. "TROPOMI ATBD Tropospheric and Total NO<sub>2</sub> Data Products." 1. 4.S5P-KNMI-L2-0005-RP.
- van Geffen, J. H. G. M., K. F. Boersma, M. van Roozendael, F. Hendrick, E. Mahieu, I. de Smedt, M. Sneep, and J. P. Veefkind. 2015. "Improved Spectral Fitting of Nitrogen Dioxide from OMI in the 405–465 Nm Window." *Atmospheric Measurement Techniques* 8 (4): 1685–1699. doi:10.5194/amt-8-1685-2015.
- Vandaele, A. C., C. Hermans, P. C. Simon, M. Carleer, R. Colin, S. Fally, M. F. Méridienne, A. Jenouvrier, and B. Coquart. 1998. "Measurements of the NO<sub>2</sub> Absorption Cross-Section from 42000 Cm<sup>-1</sup> to 10000 Cm<sup>-1</sup> (238–1000 Nm) at 220 K and 294 K." *Journal of Quantitative Spectroscopy and Radiative Transfer* 59 (3–5): 171–184. doi:10.1016/S0022-4073(97)00168-4.
- Vaughan, G., P. T. Quinn, A. C. Green, J. Bean, H. K. Roscoe, M. van Roozendael, and F. Goutail. 2006. "SAOZ Measurements of NO<sub>2</sub> at Aberystwyth." *Journal of Environmental Monitoring* 8 (3): 353–361. doi:10.1039/b511482a.
- Veefkind, J. P., I. Aben, K. McMullan, H. Förster, J. de Vries, G. Otter, J. Claas *et al.* 2012. "TROPOMI on the ESA Sentinel-5 Precursor: A GMES Mission for Global Observations of the Atmospheric Composition for Climate, Air Quality and Ozone Layer Applications." *Remote Sensing of Environment* 120:70–83. doi:10.1016/j.rse.2011.09.027.
- Vellingiri, K., K.-H. Kim, J. Y. Jeon, R. J. C. Brown, and M.-C. Jung. 2015. "Changes in NO<sub>x</sub> and O<sub>3</sub> Concentrations over a Decade at a Central Urban Area of Seoul, Korea." *Atmospheric Environment* 112 : 116–125. doi:10.1016/j.atmosenv.2015.04.032.
- Verhoelst, T., S. Compornolle, G. Pinardi, J.-C. Lambert, H. J. Eskes, K.-U. Eichmann, A.M. Fjæraa *et al.* 2021. "Ground-Based Validation of the Copernicus Sentinel-5P TROPOMI NO<sub>2</sub> Measurements with the NDACC ZSL-DOAS, MAX-DOAS and Pandora Global Networks." *Atmospheric Measurement Techniques* 14 (1): 481–510. doi:10.5194/amt-14-481-2021.
- Wang, P., A. PETERS, J. van Geffen, O. Tuinder, P. Stammes, and S. Kinne. 2020. "Shipborne MAX-DOAS Measurements for Validation of TROPOMI NO<sub>2</sub> Products." *Atmospheric Measurement Techniques* 13 (3): 1413–1426. doi:10.5194/amt-13-1413-2020.
- Wang, Y., Q. Yuan, T. Li, L. Zhu, and L. Zhang. 2021. "Estimating Daily Full-coverage near Surface O<sub>3</sub>, CO, and NO<sub>2</sub> Concentrations at a High Spatial Resolution over China Based on S5P-TROPOMI and GEOS-FP." *ISPRS Journal of Photogrammetry and Remote Sensing* 175: 311–325. doi:10.1016/j.isprsjprs.2021.03.018.
- Williams, E. J., G. L. Hutchinson, and F. C. Fehsenfeld. 1992. "NO<sub>x</sub> and N<sub>2</sub>O Emissions from Soil." *Global Biogeochemical Cycles* 6 (4): 351–388. doi:10.1029/92GB02124.
- Williams, J. E., K. Folkert Boersma, P. Le Sager, and W. W. Verstraeten. 2017. "The High-Resolution Version of TM5-MP for Optimized Satellite Retrievals: Description and Validation." *Geoscientific Model Development* 10 (2): 721–750. doi:10.5194/gmd-10-721-2017.
- Xie, Y., A. Ding, W. Nie, H. Mao, Q. Ximeng, X. Huang, X. Zheng *et al.* 2015. "Enhanced Sulfate Formation by Nitrogen Dioxide: Implications from in Situ Observations at the SORPES Station." *Journal of Geophysical Research: Atmospheres* 120:12679–12694. doi:10.1002/2015JD023607.
- Yang, K. 2017. "OMPS-NPP L2 NM Nitrogen Dioxide (NO<sub>2</sub>) Total and Tropospheric Column Swath Orbital" V. 2.0, Greenbelt, MD, USA, Goddard Earth Sciences Data and Information Services Center (GES DISC), accessed 1 June 2021], doi: 10.5067/NOXVLE2QAVR3.
- Yang, K., S. A. Carn, C. Ge, J. Wang, and R. R. Dickerson. 2014. "Advancing Measurements of Tropospheric NO<sub>2</sub> from Space: New Algorithm and First Global Results from OMPS." *Geophysical Research Letters* 41 (13): 4777–4786. doi:10.1002/2014GL060136.
- Zhao, X., D. Griffin, V. Fioletov, C. McLinden, A. Cede, M. Tiefengraber, M. Müller *et al.* 2020. "Assessment of the Quality of Tropomi High-Spatial-Resolution NO<sub>2</sub> Data Products in the Greater Toronto Area." *Atmospheric Measurement Techniques* 13 (4): 2131–2159. doi:10.5194/amt-13-2131-2020.
- Zhu, Y., Q. Hu, M. Gao, C. Zhao, C. Zhang, T. Liu, Y. Tian *et al.* 2021. "Quantifying Contributions of Local Emissions and Regional Transport to NO<sub>x</sub> in Beijing Using TROPOMI Constrained WRF-Chem Simulation." *Remote Sensing* 13 (9): 1798. doi:10.3390/rs13091798.